AN ABSTRACT OF THE THESIS OF

Thomas L. McGinnis II for the degree of Master of Science in Bioresource Engineering presented on November 6, 2001.

Title: Determining Contact Angle of Solutions with Varying Surface Tension on Dry and Pre-wetted Silica Sands.

Abstract approved: Redacted for Privacy

John S. Selker

Infiltration of highly concentrated solutions into unsaturated sand is suspected to be affected by the liquid-gas interfacial tension between the resident water and that of the infiltrating solution. The wetting of non-porous solid surfaces by liquids is commonly quantified by contact angle measurements. However, it is well known that wettability of porous solids cannot be accurately obtained by optical inspection because the liquid is penetrating into the pores of the solid in question.

The main objective of this investigation was to find an effective method to measure contact angle in coarse porous media such as sandy soils. In this study, we compare both static and dynamic methods to estimate the contact angle formed by solutions of varying surface tension on silica sands. In addition, the contact angle of the imbibing solutions is estimated in both dry and water-wetted sand.

Experiments in this study employed three clear acrylic columns of known volume to determine contact angles using two methods, one static method and one dynamic method. The three acrylic columns were packed with the same mass of each grade of Accusand® (40/50, 30/40, 20/30, and 12/20 grades respectively) for triplicate measurements. The solutions used in this study included (1) pure water and (2) 5 molal $NaNO_3$ and (3) n-hexane as a reference.

The static method estimated contact angles in initially dry sand of 23° for 40/50 sand, and 30° to 33° for 12/20, 20/30, and 30/40 sands, with the same values obtained for both solutions. Contact angles of these solutions observed in the dynamic test, were twice those found in the static test (averaging 45° and 62° respectively).

In the case of pre-wetted sands, dynamic imbibition with water provided an estimated contact angle of 2°, while the $NaNO_3$ solution yielded 21° contact. Based on relative surface tensions of water and the 5 molal $NaNO_3$, the Young's equation predicts a contact angle of 25°. These results strongly support recent claims of effective contact angles between these miscible, but contracting, fluids.

The observed data suggest that the zero contact angle assumption is a poor one even for clean dry silica sand. In a dynamic system, gravitational forces cannot be ignored in course porous media. An analytical method, used to model imbibition of the solutions into the silica sands, was both accurate and useful for estimating contact angle.

Determining Contact Angle of Solutions with Varying Surface Tension on Dry and Pre-wetted Silica Sands

by

Thomas L. McGinnis II

A THESIS

submitted to

Oregon State University

in partial fulfillment of
the requirements for the
degree of

Master of Science

Presented November 6, 2001
Commencement June 2002

Master of Science thesis of Thomas L. McGinnis II presented on November 6, 2001.

APPROVED:

Redacted for Privacy

Major Professor, representing Bioresource Engineering

Redacted for Privacy

Chair of Department of Bioengineering

Redacted for Privacy

Dean of the Graduate School

I understand that my thesis will become part of the permanent collection of Oregon State University libraries. My signature below authorizes release of my thesis to any reader upon request.

Redacted for Privacy

Thomas L. McGinnis II, Author

ACKNOWLEDGEMENTS

I would like to thank John Selker who extended me the opportunity to work with his research group on the Hanford projects and for all his helpful suggestions and assistance with the final revisions.

I cannot thank Noam Weisbrod enough for all of his help and support. His unwavering commitment to me as a friend and to this work as my professor, were very much appreciated.

I want to thank Maria Dragila and Jack Higginbotham for serving on my committee. Maria provided many helpful suggestions in the laboratory and in the first stages of writing this thesis.

I would like to thank both Michael Niemet and Mark Rockhold for their time. The success of my experiments was greatly enhanced due to Mike's technical assistance. He and Mark provided useful insight into analyzing the data compiled for this work.

A sincere thank you to all of my colleagues and friends in the Department of Bioengineering and the Department of Soil Science, who made me feel very much at home and to Nan Ritchie whose friendship and support was always very much appreciated.

I also want to thank my parents, Thomas and Carey, who have always supported me in any way possible to achieve my goals.

TABLE OF CONTENTS

TABLE OF CONTENTS (CONTINUED)

LIST OF FIGURES

LIST OF FIGURES (CONTINUED)

LIST OF FIGURES (CONTINUED)

LIST OF FIGURES (CONTINUED)

LIST OF TABLES

This thesis is dedicated to the memory of my grandfathers:

Bernard Carlton McGinnis, Jr., a wonderful man whose untimely death prevented our relationship from growing beyond my early childhood.

Henry Drury Hatfield, for his larger-than-life sense of humor, for teaching me to play golf, and many fond memories.

and

Clarence H. Pratt, second husband to my grandmother Muriel, and in every sense, fulfilled the role of a wonderful grandfather.

DETERMINING CONTACT ANGLE OF SOLUTIONS WITH VARYING SURFACE TENSION ON DRY AND PRE-WETTED SILICA SANDS

1 INTRODUCTION

Wettability refers to the response evinced when a liquid is brought into contact with a solid surface initially in contact with a gas or another liquid (Blake, 1993). The wetting of solid surfaces by liquids and the ultimate extent of spreading of that liquid are very important processes to consider for many industrial applications. For example, everyone from furniture to car manufacturers needs to know how well paints and polymeric coatings protect finishes and repel solvents. The pharmaceutical industry is concerned with wetting of biological fluids. The degree to which lubricants wet and adhere to working metal surfaces is important to engine and machinery manufacturers. "Wetting", by definition, is the process of one fluid displacing another fluid at a solid surface. However, in most cases, the term is used to describe the displacement of air by a liquid (Rulison, 1996a). The wetting of non-porous solid surfaces by liquids is commonly quantified by measurement of the contact angle of the advancing liquid on the solid surface. The liquid may move out over the solid, displacing the original fluid, and finally coming to a halt when the angle between the liquid-fluid and solid-liquid interfaces reaches mechanical equilibrium (Blake, 1993). On the other hand, the liquid may spread without limit, displacing the original fluid from the entire solid surface area available, a situation evidently corresponding to a contact angle of 0° (Blake,

1993). Contact angle also controls the spontaneous imbibition of liquids into porous media (Blake, 1993). The smaller the contact angle of the advancing liquid on a surface, the more susceptible to wetting the solid is. Alternatively, the larger the contact angle that the advancing liquid forms on a surface, the less susceptible the solid is to wetting by the fluid.

1.1 THE CONTACT ANGLE

When a drop of liquid is placed on a solid surface, the liquid will either spread across the surface to form a thin layer or will remain as a distinct drop on the surface. The final condition of the applied liquid on the surface is taken as an indication of the wettability of the surface by the liquid or the wetting ability of the liquid on the surface, depending on your point of view (Meyers, 1991). A quantitative measure of this wetting process is the contact angle, which the drop of liquid makes against the planar surface of the solid onto which it is applied (Figure 1.1).

When the contact angle is zero, the liquid forms a film, and the solid is completely wetted by the liquid. Where a non-zero contact angle is formed, there exists some controversy as to how to describe the system (Meyers, 1991). Partially wetted systems (hydrophilic) yield contact angles between 0° and 90°, while contact angles on hydrophobic surfaces are above 90° and are considered nonwetting (Figure 1.2 and 1.3).

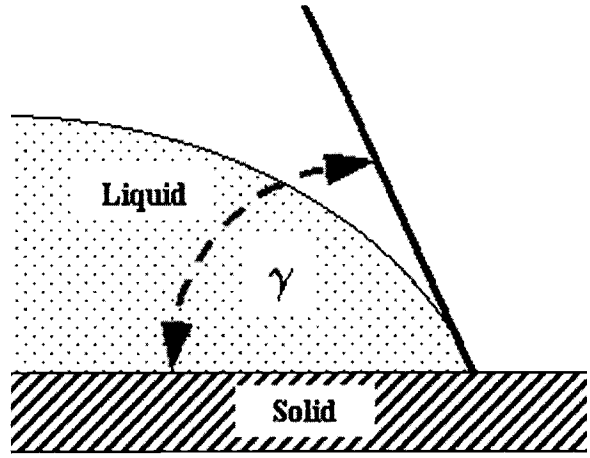

Figure 1.1 The contact angle γ formed by a liquid drop on a solid surface illustrated.

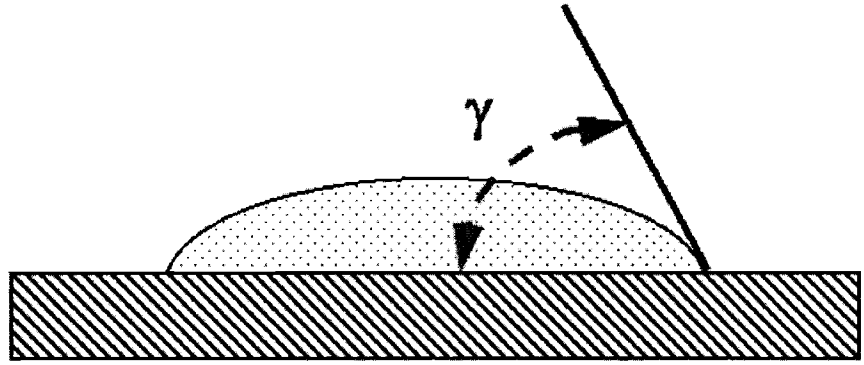

Figure 1.2 Sessile drop reaction on a hydrophilic solid. Here the contact angle γ is approximately 60°.

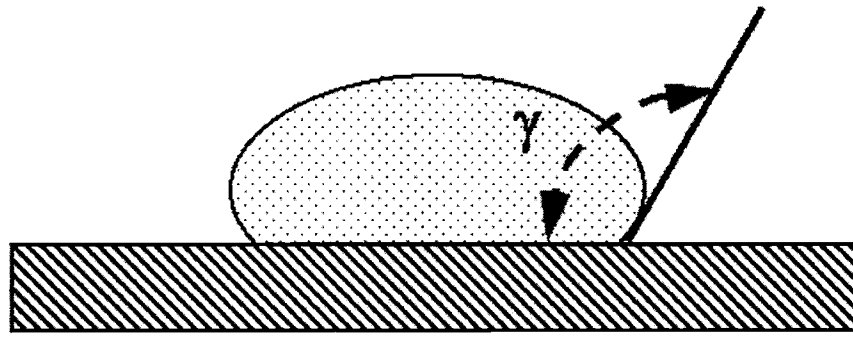

Figure 1.3 Sessile drop reaction on a hydrophobic solid. Here the contact angle γ is approximately 130°.

Table 1.1 List of Symbols and their meaning.

Symbol	Definition	Symbol	Definition
γ	Contact angle	h_f	Pressure potential at the wetting front interface
γ_A	Advancing contact angle	K_S	Saturated hydraulic conductivity of the soil
γ_R	Receding contact angle	K_{FS}	Saturated hydraulic conductivity of the soil as fitted by Green and Ampt
F_{lg}	Liquid/gas surface force	d_p	Depth of ponding on the surface
F_{sl}	Solid/liquid surface force	v	Velocity
F_{sg}	Solid/gas surface force	L	Length of liquid inside a capillary
F	Total force felt by a solid	H	Hydraulic head difference
F_b	Buoyant component of force	H_1	Hydraulic head at point one
σ_{lg}	Liquid/gas interfacial tension	H_2	Hydraulic head at point two
σ_{sl}	Solid/liquid interfacial tension	x	Length of sample
σ_{sg}	Solid/gas interfacial tension	dV	Change in volume of water passing through the sample
P	Pressure	dt	Amount of time elapsed

Table 1.1 (Continued)

Symbol	Definition	Symbol	Definition
P_0	Atmospheric pressure	t_1	Starting time
P_l	Liquid pressure	t_2	Finishing time
P_v	Pressure in the gas phase	a	Cross-sectional area of the standpipe
n	porosity	A	Cross-sectional area of the sample
P_g	Pressure due to gravitational forces	q	Flux
P_c	Pressure due to capillary forces	κ_S	Intrinsic permeability relative to the measured K_S of the soil.
h	Height of capillary rise	κ_{FS}	Intrinsic permeability relative to the fitted K_{FS} by Green and Ampt.
r	Effective capillary radius	w	Gravimetric water content
ρ_l	Density of liquid	M_w	Mass of water
ρ_g	Density of gas	M_s	Mass of sand
d	Depth below free surface	θ_v	Volumetric water content
g	Gravitational constant of acceleration	ρ_b	Bulk density of the soil
R	Radius of curvature	ρ_w	Density of water
V_T	Total volume of sample column	r_b	Radius of a pore body
V_S	Total volume of sand	r_n	Radius of a pore neck
V_l	Total volume of liquid	θ	Degree of saturation
R_c	Radius of sample column	θ_0	Residual saturation
m_l	Mass of liquid	θ_S	Full saturation
Φ	Liquid content	θ_{fs}	Fitted degree of saturation
π	Pi (3.14...)	η	$2/\lambda+3$
t	Time	λ	Fitting parameter for a given media
t_0	Initial time of imbibtion	$K(\theta)$	Hydraulic conductivity at a given degree of saturation
μ_l	Dynamic viscosity of liquid	$P_\bullet$	Scaled pressure
A	Constant representing the liquid/solid properties	$h_\bullet$	Scaled pressure head
		$r_\bullet$	Scaled pore radius

The contact angle may be geometrically defined as the angle formed by the intersection of the two planes tangent to the liquid and solid surfaces at the perimeter of contact between the two phases and the third surrounding phase. Typically the third phase will be the gas phase. The perimeter of contact among the three phases is commonly referred to as the three-phase contact line (Figure 1.4) or the wetting line (Meyers, 1991).

Consider only the component of forces acting in the horizontal direction,

$$\sum F = 0 = F_{sl} - F_{sg} + F_{\mathrm{lg}} \cos\gamma \tag{1.1}$$

where F_{sg} is the solid/gas surface force per unit length, F_{sl} is the solid/liquid surface force, F_{lg} is the liquid/gas surface force, and γ is the contact angle. Per unit length $F_{ij}=\sigma_{ij}$, so this may be put in terms of the relative surface tensions:

$$\sigma_{sg} = \sigma_{sl} + \sigma_{\mathrm{lg}} \cos\gamma \tag{1.2}$$

which is known as the Young-Laplace equation (Selker et al., 1999). Solving Equation (1.2) for the contact angle yields

$$\gamma = \cos^{-1}\left(\frac{\sigma_{sg} - \sigma_{sl}}{\sigma_{\mathrm{lg}}}\right) \tag{1.3}$$

One should keep in mind that the intimate situation at this three-phase line is a sensitive transition zone where the phases merge and where the interfaces may not be as sharp as that depicted in the conceptual model of Figure 1.4.

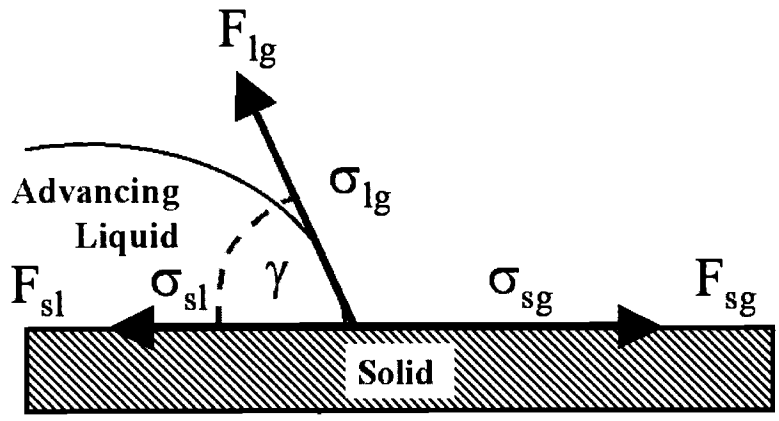

Figure 1.4 Three-phase line of contact between forces. Here F_{sg} is the solid/gas surface force per unit length, F_{lg} is the liquid/gas surface force, F_{sl} is the solid/liquid surface force, σ_{sg} is the relative surface tension between the solid and the gas, σ_{lg} is the relative surface tension between the liquid and the gas, and σ_{sl} is the relative surface tension between the solid and the liquid. The γ term denotes the contact angle.

While it may be mathematically convenient to think of this zone in terms of lines, the reality of complex curvature in materials with heterogeneity at all scales should be kept in mind, particularly when defining contact angle measurements using a dynamic method.

It has been observed in dynamic systems that contact angle varies as a function of the velocity of the wetting front, with the advancing contact angle increasing with velocity and the receding contact angle decreasing (Figure 1.5) (Meyers, 1991). In the wetting process, available energy is dissipated, may be as a result, the advancing contact angle is intrinsically higher than the receding one (Yang, 1995).

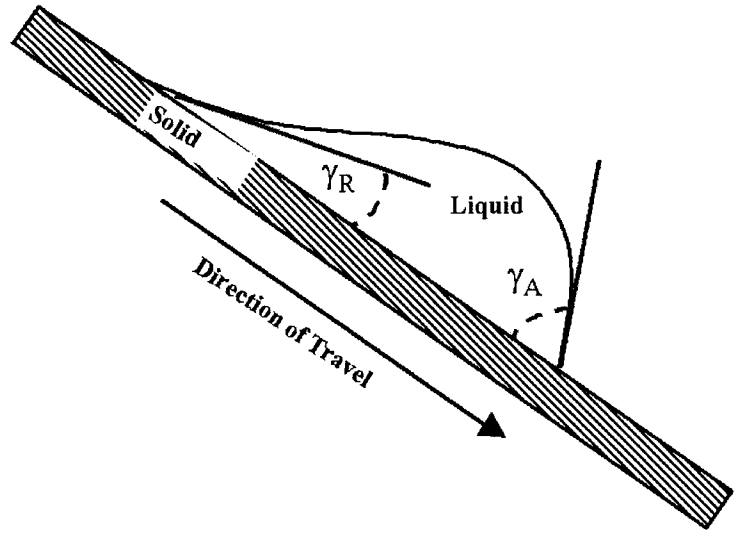

Figure 1.5 The difference in advancing γ_A and receding γ_R contact angle. As the velocity in the direction of travel increases, the γ_A will increase while the γ_R will decrease.

1.2 DETERMINING CONTACT ANGLE

There are a variety of simple and inexpensive techniques for measuring contact angles. The most common and direct methods include the sessile drop (Figure 1.6a), the captive bubble (Figure 1.6b), the sessile bubble (Figure 1.6c), and the tilting plate (Figure 1.6d). These methods are such that the contact angle can be directly observed visually or with the aid of image analysis software. Indirect methods include tensiometry and geometric analysis of the shape of the meniscus.

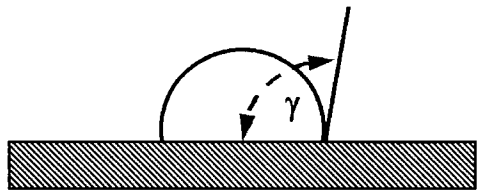

Figure 1.6a Sessile drop

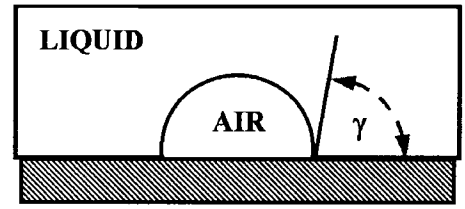

Figure1.6b Captive bubble

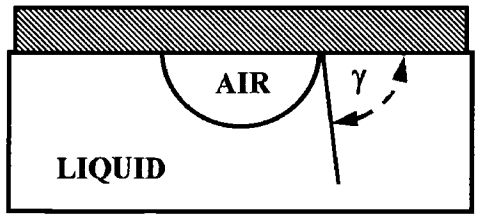

Figure 1.6c Sessile bubble

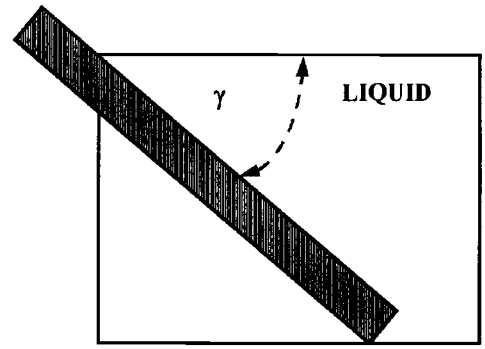

Figure 1.6d Tilting plate

Figure 1.6 Most common simple and inexpensive methods for measuring contact angle.

Two popular methods to measure contact angle on solid surfaces are the goniometer method and the Wilhelmy method. The goniometer method is the more straightforward of the two. Advancing contact angles can be determined using the goniometer by placing a drop of liquid on the surface. The drop is advanced on the solid surface by increasing its volume (Figure 1.7). The contact angle is measured visually at a grazing angle or by image analysis. Receding contact angles can be determined in a similar manner by contracting a drop of a certain volume (Figure 1.8). As the drop is contracted, the angle is measured again by inspection or image analysis.

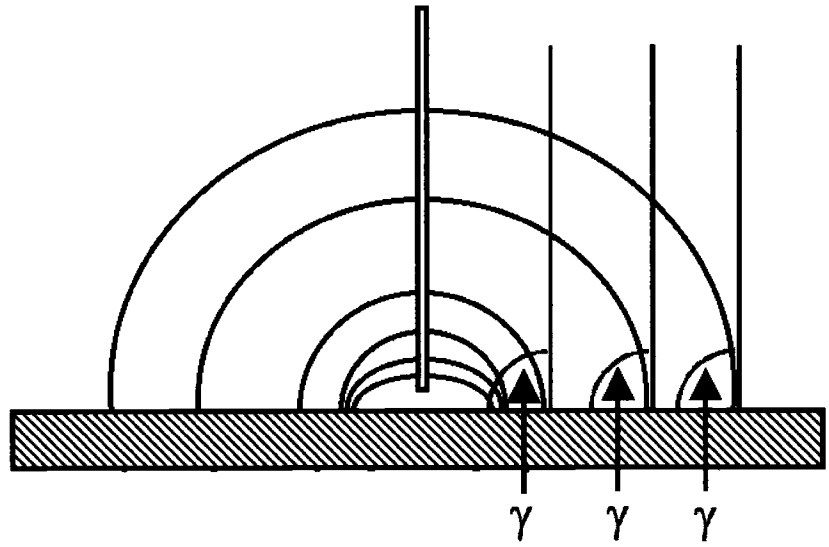

Figure 1.7 Goniometer method used to measure the advancing contact angle of a liquid drop on a solid plane. The drop is applied through the capillary tube and the volume increased. The contact angle formed by the advancing liquid on the solid is observed at varying increments.

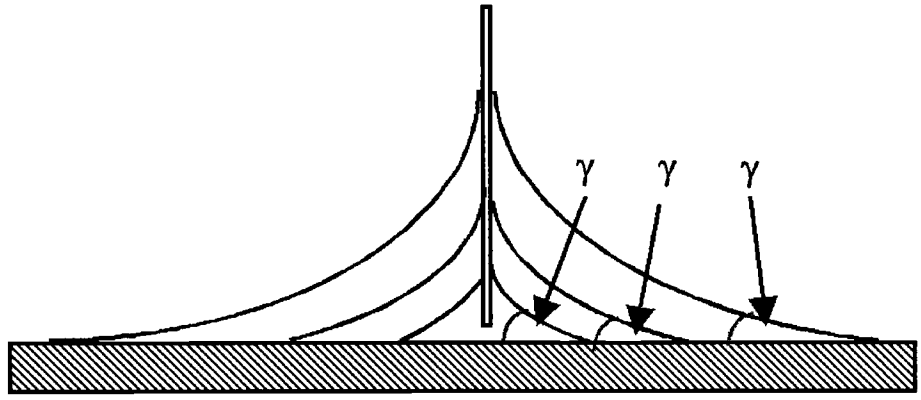

Figure 1.8 Goniometer method used to measure the receding contact angle of a liquid drop on a solid plane. The drop is applied through the capillary tube and the volume of that drop retracted by suction. The contact angle formed by the retreating liquid on the solid is observed at varying increments.

In the goniometer method, the contact angle is observed directly, while in the Wilhelmy method, the contact angle is calculated from force data using the Wilhelmy equation

$$\cos\gamma = \frac{F - F_b}{I\sigma} \tag{1.4}$$

where F is the total force felt by the solid at any submersion position, F_b is the buoyant component of the force on the solid at any submersion position, I is the sample's wetted length, and σ is the surface tension of the liquid. F_b is due to the solid displacing the liquid as it is submerged and removed. The advancing contact angle of a liquid on a solid is determined from force data obtained during submersion of the solid into the liquid. The receding contact angle is likewise determined from force data pertaining to the removal of the solid from the liquid (Figure 1.9). Each method has its advantages and disadvantages, and the method of choice is largely dependent on the research application.

1.3 POROUS SOLIDS

The wettability of porous materials such as textiles, paper, and powders are also important to industry. Natural sediments also form porous media. Therefore contact angles developed by an advancing liquid in soils or aquifer sediments can be important in subsurface transport processes. The wetting of porous solids however, presents certain physical constraints that render more traditional types of contact angle measurement largely inapplicable. The contact angle of a liquid

cannot be obtained by optical inspection if a liquid is penetrating into the pores of an opaque solid. Likewise, any penetration of liquid into the pores of the solid during an experiment employing the Wilhelmy plate method, causes an error in force which is difficult, at best, and impossible, at worst, to correct for (Rulison, 1996b). For solids such as powders and porous materials, methods based on capillary pressures and imbibition rates have been developed (Meyers, 1991).

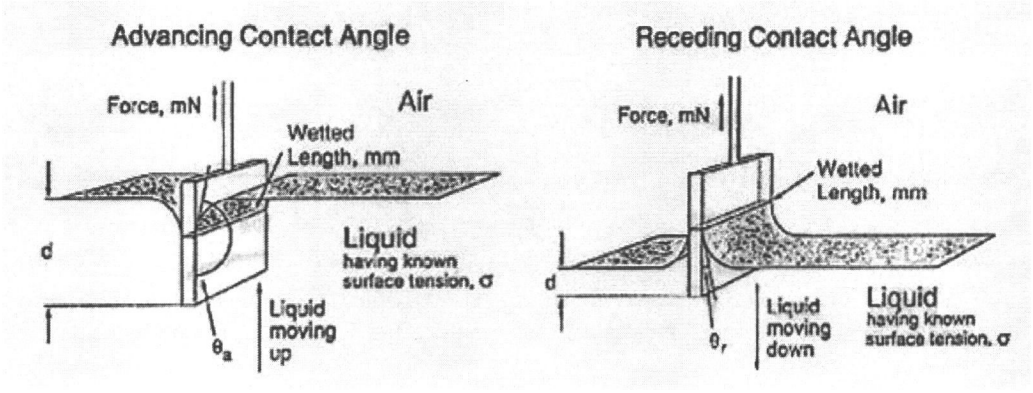

Figure 1.9 Wilhelmy plate method used to measure advancing and receding contact angles. The net of the directional force minus the solid's buoyant force is measured while acting on a solid of known length in a liquid of known surface tension. In this figure only, θ denotes the contact angle (Rulison, 1996a).

1.4 MEASURING CONTACT ANGLE IN SOILS

Soils do not provide planar surfaces that allow the geometric measurement of a contact angle. Thus, an alternative to geometric measurement is required (Letey et al., 1999). The simplest model that has been extensively studied is the cylindrical capillary (Marmur, 1992). Soils have pores and often have been conceptualized as

being composed of a bundle of capillary tubes (e.g. Green and Ampt, 1911, and Letey et al., 1999).

The capillary tube dipped in a body of free water will form a meniscus as the result of the contact angle with the walls of the tube (Hillel, 1998) (see Figure 1.10). The curvature of this meniscus will be greater (i.e., the radius of curvature smaller) the narrower the tube (Hillel, 1998). This curvature causes a pressure change across the gas-liquid interface. A liquid with a contact angle of less that 90° (as such water forms on glass) will form a concave meniscus as shown in Figure 1.10. Therefore, the liquid pressure under the meniscus P_l will be smaller than the atmospheric pressure P_0. Thus, the water inside the tube, as well as the meniscus, will be driven up the tube from its original location (shown as a dashed line in Figure 1.10). The greater pressure of the free liquid outside the tube at the same level is the initial driving force and continues to force the liquid up the tube until the pressure drop between the liquid inside the tube and the liquid under the free surface outside the tube is equal and opposite to the hydrostatic pressure exerted by the water column in the capillary tube.

Assuming that the capillary tube is cylindrical and the contact angle of the liquid on the walls of the tube is zero, the meniscus will be a hemisphere (and in a two-dimensional drawing can be represented by a semicircle) with its radius of curvature equal to the radius of the capillary tube (Hillel, 1998). When the contact angle that the liquid creates on the wall of the tube is between 0° and 90°, the diameter of the tube $2r$ is the length of a chord cutting a section of a circle with an

angle of π - 2γ, as shown in Figure 1.11. Here R is the radius of curvature of the meniscus, r the radius of the capillary, and γ the contact angle. The difference in pressure at a point between the capillary liquid under the meniscus and the atmosphere at equilibrium is

$$\Delta P = P_v - P_l = \frac{2(\sigma_{sg} - \sigma_{ls})}{r} \tag{1.5}$$

where ΔP is the change in pressure across the gas-liquid interface, P_v is the pressure in the gas phase, P_l is the pressure in the liquid phase, σ_{sg} is the interfacial tension of the solid-gas interface, and σ_{ls} is the interfacial tension of the liquid-solid

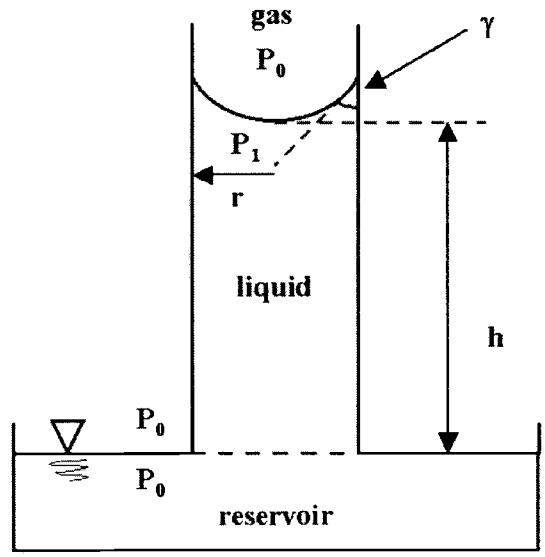

Figure 1.10 The classic capillary model. As the capillary tube is touched to the surface of liquid in a reservoir, it climbs from its original position (denoted by the dashed line) to some height h. Atmospheric pressure is denoted by P_0. The liquid pressure under the meniscus is represented by P_l and the radius of the capillary is r. The contact angle formed by the liquid on the capillary wall as shown is γ.

interface. For most systems, the interfacial tensions, σ_{sg} and σ_{ls}, cannot be measured accurately. Therefore it is typically sought to express Equation 1.5 in terms of readily available parameters. In most gas-liquid-solid capillary systems these parameters are the liquid-gas interfacial tension and the contact angle between the liquid-gas interface and the solid.

Young's equation (Equation 1.2) states that for contact between a liquid-gas interface and rigid solid at equilibrium, the interfacial tension at the solid/gas interface is equal to the interfacial tension at the liquid/solid interface plus the interfacial tension at the liquid/gas interface multiplied by the cosine of the contact angle formed by the liquid on the solid. Combining Equations 1.2 and 1.5 yields the classical form of the Laplace equation for pressure across a spherical fluid interface in a capillary tube, that is to say pressure due to capillary forces is given by

$$P_c = \frac{2\sigma_{\mathrm{lg}} \cos\gamma}{r} \tag{1.6}$$

Recalling that hydrostatic pressure is proportional to the depth d below the free surface, we can infer that the hydrostatic tension (negative pressure) in a capillary tube is proportional to the height h above the free water surface. Therefore pressure due to gravitational force is given by

$$P_g = \rho_l g h \tag{1.7}$$

where ρ_l is the liquid density and g is the gravitational constant of acceleration (9.81 m/sec^2). Hence the height of capillary rise is

$$h = \frac{(2\sigma_{lg}\cos\gamma)}{(\rho_l - \rho_g)gr} \tag{1.8}$$

where ρ_g is the density of the gas (which is generally neglected). We use the capillary pressure model in our unsaturated porous media to calculate the contact angle.

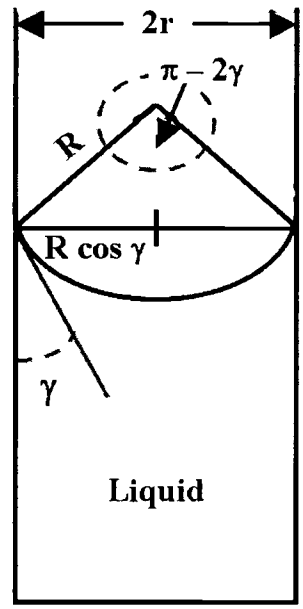

Figure 1.11 The geometric relationship of the radius of curvature R to the radius of the capillary r and the contact angle γ.

1.5 INTERFACIAL TENSION

Interfacial tension, or surface tension, is an important parameter affecting infiltration in unsaturated porous media (Weisbrod et al., submitted a). Selker and

Schroth (1998) found that the effective contact angle of liquid entering dry sand was far from zero, and confirmed that Miller scaling cannot be used to account for the effect of liquid-air interfacial tension. There have been studies of those mechanisms that control infiltration of high strength saline solutions, which may have significantly higher surface tensions than water (Weisbrod et al., submitted a). Previous works involving saline solutions have been considered in model systems by Ouyang and Zheng (1999), where the impacts of solution density was investigated and found to be negligible. Possible impacts from infiltrating solutions with surface tension higher than pure water and the contact angle of these solutions was however neglected.

1.6 DETERMINATION OF CONTACT ANGLE IN SOILS

Most previous efforts to determine contact angle in soils have involved the use of the vertical capillary model as a tool to solve for the contact angle. Letey et al. (1962) reported a technique for measuring water-solid contact angle for soils using such a capillary rise approach. The authors assumed that ethanol (surface tension of 22.5 mN/m) wets all soil with a contact angle equal to zero. This assumption was used by Letey et al. (1962) and Tillman et al. (1989) to determine contact angle in soils treated with water repellent materials. Tillman et al. (1989) measured sorptivity of water and ethanol in soil columns and used the ratio of ethanol to water sorptivity as a repellency index. Letey et al. (1962) measured infiltration rates of ethanol and water into soil columns to measure the water-solid contact

angles. In related studies, solutions of low surface tension such as ethanol (σ_{lg} = 22.5 mN/m) and n-hexane (σ_{lg} = 18.4 mN/m) were used to calculate the capillary radius r via the following equation

$$r = \frac{2\sigma_e \cos\gamma_e}{\rho_e g h_e} \tag{1.9}$$

where the subscript e denotes ethanol with assumed contact angle of zero. The parameters are readily known or measured and the cosine of 0° is one, thus the average pore radius specific to the soil is easily calculated. Once determined, this geometric constant r, which is unique to the media, can be substituted back in to Equation 1.9. Rearranging terms and changing the parameters to those pertaining to the imbibing liquid (e.g. water), the contact angle that liquid has on the dry soil can be estimated via

$$\cos\gamma_w = \frac{\rho_w g r h_w}{2\sigma_w} \tag{1.10}$$

where w denotes water.

These indirect procedures circumvent the need for a geometric measurement of contact angle, which is impossible in soils (Letey et al., 1999). The method employed by Letey et al. (1962), is known as a static method in which the contact angle is measured at an equilibrium state within the system, achieved when the height of capillary rise is deemed to have reached equilibrium. In a static system, the effects of temporal changes that take place during imbibition are not seen. Letey et al. (1962) notes that equilibrium time was assumed to be 24 hours in each

case, because further rise, if any at all, was extremely slow. Table 1.2 below summarizes the contact angle values determined by Letey et al. (1962) for water formed on beach sand and pure quartz. Each type of sand was washed and then treated to alter its wettability in the first three repetitions. The treatments consisted of (a) NH_4OH extract of chaparral litter, (b) water extract of chaparral litter, and (c) NH_4OH-starch solution, all separately mixed with the sands and allowed to dry (Letey et al., 1962). By looking at the data in Table 1.2, one could observe that the treated sands are more hydrophobic due to the larger contact angle that was calculated from the height of capillary rise.

Table 1.2 Contact angle measurements for a range of sands, treated and untreated from *Letey et al. (1962).*

Sand Size	Contact Angle			
	NH_4OH + chaparral	H_2O + chaparral	NH_4OH + Starch	Untreated
Quartz:				
28-32 mesh	84°	76°	78°	52°
32-48 mesh	83°	72°	76°	43°
48-65 mesh	83°	72°	76°	43°
Unsieved	82°	77°	-	47°
Beach Sand:				
48-65 mesh	81°	64°	73°	51°
65-100 mesh	81°	60°	72°	46°
Unsieved	84°	64°	69°	52°

Different static measurement methods for determining contact angle have been used in other research areas. One issue that has received much attention involves using measurement techniques that quantify the degree of soil water repellency for

agricultural use of pesticides. The water drop penetration time (WDPT) is a commonly used measurement (Letey et al., 1999). This procedure involves placing a drop of water on the soil and measuring the time it takes to penetrate. The liquid surface tension, which wets the soil material with a 90° contact angle was proposed as an index of water repellency by Watson and Letey (1970). This procedure employs the concept that a liquid can only completely enter the soil if the contact angle is less than 90° (Letey et al., 1999). Bauters et al. (2000) used WDPT to observe apparent contact angles in sandy soils of differing hydrophilic and hydrophobic properties (Bauters et al., 2000). Water on slightly water repellent sands using this method had an apparent contact angle of 67° (Bauters et al., 2000). This value is close to the 51.7° contact angle found for water entering a capillary tube of 0.03 cm radius (Malik et al., 1979). However in this research Bauters et al. (2000), employed the assumption that the hydrophilic soil has a contact angle of 0°, which is debatable.

An evaluation of the effective contact angle of fluids on sand was made by Selker and Schroth (1998). Their experimental results demonstrated effective contact angles approaching 60° in clean silica sand. In a microscopic grain-wise study, Selker and Schroth (1998) found that twelve of the twenty-six sand grains tested had a nonzero contact angle with pure water, six continued to have nonzero contact angle with 0.001 M sodium dodecyl sulfate surfactant solution, and five had nonzero contact angle with 0.006 M sodium dodecyl sulfate surfactant solution. These results are consistent with fingered flow experiments, which suggest that

contact angle is nonzero for pure water and that a decreasing gas-liquid interfacial tension does reduce the effective contact angle (Selker and Schroth, 1998).

In addition to the extensive literature on static contact angle measurement employing the capillary model, dynamic methods for determining contact angle have also been used. These efforts began with Edward Washburn, who examined and mathematically quantified the dynamics of capillary flow in 1921, resulting in what is known today as the "Washburn Equation" or "Washburn Theory" (Washburn, 1921). The Washburn theory indicates that if a porous solid is just brought into contact with a liquid, then the rise of liquid into the pores of the solid due to capillary action will be governed by the Washburn equation (Rulison, 1996b). In capillary systems in which liquid flow is relatively fast, the effects of a dynamic advancing contact angle may become apparent (Meyers, 1991). In dynamic systems, the advancing contact angle measured will be greater than that of a static system (Meyers, 1991). The advancing contact angle measured in a dynamic system will generally be found to increase with speed of liquid flow. In systems of large-bore, short path capillaries or those with a high static advancing contact angle, the effects of the dynamic contact angle on liquid movement may appear at relatively slow flow rates (Meyers, 1991). In dynamic contact angle studies, additional complications arise because the movement of the wetting line is not always a steady, continuous process. It is often observed that the movement is abrupt, with the drop or liquid front holding a position for a time and then jumping to a new configuration. This phenomenon is often referred to as a "stick—slip"

process and is not fully understood (Meyers, 1991). This is also referred to as "Haines jumps" after Haines (1930) pointed out that unsaturated porous media could have a variety of moisture contents at a given capillary pressure depending on the history of wetting. This process is known as hysteresis. Haines pointed out that even in an idealized media the advancement (or retreat) of fluid into porous media was a highly nonlinear process, proceeding in a sequence of "jumps" as the fluid proceeds (or recedes) from pore to pore. It has been observed in other research in dynamic systems, that the values of the advancing and receding contact angles vary as a function of the velocity of the wetting front, with the advancing contact angle increasing with velocity and the receding contact angle decreasing (Fisher and Lark, 1979), (Marmur, 1992), (Meyers, 1991), and (Schaffer, 2000). Most dynamic contact angle research and measurement has been conducted on flat solids or in capillary tubes. Applying these methods to soils has not been addressed except in the context of capillary tubes, and using the assumption that a soil can be represented approximately by a bundle of capillary tubes.

1.7 RELEVANCE OF THIS RESEARCH

Infiltration of highly saline solutions is likely to be of concern in selected landfills, industrial complexes and other facilities (Weisbrod et al., submitted a). One such extreme case is the Hanford Nuclear Reservation in southeast Washington State, which is home to several underground storage tank farms of radioactive wastes. Over the last 50 years, large volumes of these highly saline

solutions have leaked into the unsaturated zone beneath the tanks. Unlike agrochemicals and other contaminants, these caustic solutions are extremely saline. These solutions, with salinity concentrations exceeding 5 mole/L, have been identified in the local groundwater system at a depth of roughly 60 meters below the ground surface in some areas (GJPO, 1996). Among other significant factors affecting the infiltration of these solutions (density, viscosity, surface tension) the contact angle between the advancing saline solutions and the interface with which it is wetting is an important parameter.

1.8 OBJECTIVES

The primary objective of this study was to determine if different contact angles develop for pure water and saline solution during infiltration into porous media. Specific objectives include: (1) Comparison between static and dynamic methods of contact angle measurement; (2) Find and utilize a model to describe the observed behavior of the wetting front; and (3) Compare the contact angle developed by pure water and that of the saline solution in air-dry and pre-wetted sand. The objective in using pre-wetted (but unsaturated) sand was to create a more realistic environment for the imbibing solutions being tested, as we know that even sandy soils carry a percentage of residual water. Many issues are raised when applying accepted capillary theories to pre-wetted soils. Issues including the change in effective pore radius, which is the amount of pore space available for imbibing fluid once the sand grains are coated with water films, are among the most

important. By applying the capillary theories discussed, one would expect to see the balance of forces and interfacial tension along the three-phase contact line illustrated. Based on the physical phenomenon of wetting hysteresis, one would hope to see the measured contact angle formed by water on pre-wetted sand very close to 0°. This research provides some insight into the many intricacies, which evolve when applying accepted capillary theories to soils. Even though the goal was to achieve a concise and reliable method for measuring and understanding the influence of contact angle during the infiltration of saline solutions into pre-wetted sand, possible reasons why these methods may be applicable to initially dry sand and not to water-wetted sand are addressed.

2 MATERIALS AND METHODS

2.1 THEORY

2.1.1 Static Method

Two capillary rise methods were used in the contact angle experiments. The first, which we call the static method was adapted from Letey et al. (1962). The capillary pressure P_c and the gravitational pressure P_g are taken to be in equilibrium when the system is at steady state. The Laplace equation (Equation 1.6) is used to compute the pressure due to capillary forces. The pressure due to gravity is computed via (Equation 1.7). At equilibrium, the two pressure components are equal

$$P_g = P_c \tag{2.1}$$

The effective capillary radius r can be obtained by equating Equations 1.6 and 1.7 to yield

$$r = \frac{2\sigma_{lg}\cos\gamma}{\rho_l g h} \tag{2.2}$$

It should be noted however, that the assumption of a single capillary radius is artificial, since the structure of natural porous media is very complex with a broad distribution of pore sizes. The concept here is that if we can measure a height of

capillary rise in the same media with two different fluids, that we can use the same value of r in both cases, and solve for the change in contact angle.

To obtain r for a specific media, we employ a liquid with a 0° contact angle. Since σ_{lg}, ρ_l, g and h are known or can be measured, we may solve Equation 2.2 for r. N-hexane was used for the imbibing solution because it wets quartz with an apparent contact angle 0° at room temperature, in part due to its low surface tension (σ_{lg} =18.4 mN/m) (Rulison, 1996b). The zero contact angle was verified using 40/50 grade Accusand® packed into vertical light transmission chambers as described by Niemet and Selker (2001). The chamber was allowed to imbibe n-hexane using a Marriot bottle source to provide a constant pressure, lower boundary condition of P=0. After allowing the n-hexane to imbibe overnight, an image was taken and the height of rise noted (approximately 3.5 cm). The Marriot bottle was then raised enough to allow the chamber to fully saturate. At this point, the Marriot bottle was removed from the system and the chamber was allowed to freely drain overnight, at which point another image was taken. Subtracting the initial imbibition image from the drained image yielded virtually no difference in height between the height of rise and the capillary fringe. Measuring directly from the chamber yielded a difference of less than 0.5 cm.

Since the density and surface tension of a given solution can be easily determined, only two unknowns are left, h and γ. The height of rise of the imbibing solution h into the porous media is readily calculated by considering the following relationship:

$$V_l = \pi R_c^{\,2} hn \tag{2.3}$$

where R_c is the radius of the column, and n is the porosity of the packed media. The volume of the liquid imbibed, V_l, is given by

$$V_l = \frac{m_l}{\rho_l} \tag{2.4}$$

where m_l is the mass of the liquid imbibed as measured experimentally. The porosity is given by

$$n = \frac{\left(V_T - V_S\right)}{V_T} \tag{2.5}$$

where V_T represents the volume of the column (directly measured) and V_S the volume of the sand in the column (obtained by measured weight and known particle density). With Equation 2.4 and 2.5, Equation 2.3 can now be solved for h. With this and r, the only unknown in Equation 2.2 is the contact angle γ:

$$\gamma = \cos^{-1}\left(\frac{\rho_l grh}{2\sigma_{\mathrm{lg}}}\right) \tag{2.6}$$

2.1.2 Dynamic Method

The second method for measuring contact angle in dry sand, referred to here as the dynamic method, is derived from the Washburn theory (Washburn, 1921). The theory indicates that if a porous solid is brought into contact with a liquid (not

submerged), then the imbibition of liquid into the pores of the solid due to capillary action (ignoring gravity) will be governed by

$$t = Am_l^2 \tag{2.7}$$

where t is the time after the solid and the liquid are brought into contact, m represents the mass of liquid imbibed. A is a constant which is dependent on the properties of the liquid and the solid in question. Specifically,

$$A = \frac{\mu_l}{c\rho_l^2 \sigma_{\text{lg}} \cos\gamma} \tag{2.8}$$

where μ_l is the dynamic viscosity of the liquid, and c is a material constant which is dependent on the specified media type used in the experiment. By combining and rearranging Equations 2.7 and 2.8 one may solve for the contact angle (Rulison, 1996b).

$$\cos\gamma = \frac{m_l^2}{t}\frac{\mu_l}{\rho_l^2 \sigma_{\text{lg}} c} \tag{2.9}$$

The density, viscosity, and surface tension of the liquid are assumed known. The mass of liquid that rises into the sand is measured with time.

As in the static method, n-hexane was used in order to determine the constant c for the porous media tested. In this case, since the contact angle γ is zero, c is the only unknown and can be determined using Equation 2.9. Once the material constant was determined for a particular grade of sand, a second sample of that sand packed in a similar fashion was tested for wettability by another liquid. Although taken as a constant here, it should be noted that since contact angle is a

function of the rate of wetting, in this method γ is strictly speaking, a time dependent parameter, as imbibition rates vary within each experiment and between the different sand grades.

2.1.3 Analytical Method

The one-dimensional infiltration model developed by Green and Ampt in 1911 provides a useful framework for the characterization of imbibition driven by capillary wetting (Green and Ampt, 1911). The basic assumptions for this approach are that the wetting front is sharp, provides a driving force h_f, and is at a well-defined position. For the Accusand®, this model was applied to the raw data from the dynamic experiments. Dry sandy soils typically exhibit a sharp wetting front, conforming well to the Green and Ampt assumption. The effects of gravity, which were deficient in the original Washburn method, are readily incorporated here (Section 2.1.2).

The Green and Ampt result for ponded downward imbibition is given by Selker et al. (1999).

$$\frac{d}{dt} nh = K_S \left[\frac{h_f + d_p + h}{h} \right] \tag{2.10}$$

where h is the depth of infiltration, h_f is the pressure potential at the wetting front, d_p is the depth of ponding on the surface, and K_S is the saturated hydraulic conductivity of the soil. In our experiments d_p can be dropped since there is no

ponding, and a sign convention was changed in order to reflect vertical upward imbibition of our system, yielding

$$\frac{dh}{dt} = \frac{K_S}{n}\left[\frac{h_f - h}{h}\right] \tag{2.11}$$

The microscopic scale equation for the kinetics of imbibition was developed by Lucas and Washburn (Marmur, 1992). They assumed a quasi-steady state, fully developed laminar flow of a Newtonian fluid (a fluid for which the shear stress is directly proportional to the rate of strain), with negligible inertia effects. Therefore, the average velocity v was calculated from the Hagen-Poiseuille equation:

$$v = \frac{dL}{dt} = \frac{r^2}{8\mu_l}\left(\frac{\Delta P}{L}\right) \tag{2.12}$$

where L is the length of the liquid inside a capillary tube and ΔP is the pressure difference across the liquid.

The driving force for penetration comes from the pressure difference across the liquid, which can be expressed as the pressure due to capillary forces minus the pressure due to gravity:

$$\Delta P = \frac{2\sigma_{lg}\cos\gamma}{r} - \rho_l g h \tag{2.13}$$

The pressure terms in Equations 2.11 and 2.12 are similar, thus the other part of these equations, K_S/n in Equation 2.11 and $r^2/8\mu_l$ in Equation 2.12, are also similar in that they are unique properties of the media. This leaves us with similar

terms for a single capillary as found using the Hagen-Poiseuille (Equation 2.12) and the Green and Ampt (Equation 2.11) description of bulk porous media.

2.2 EXPERIMENTAL PROCEDURE

2.2.1 Sand

The media used was Accusand® (Unimin, Le Sueur, MN) silica sands in 40/50, 30/40, 20/30 and 12/20 grades. Important physical and mineralogical properties of the sand are summarized in Table 2.1. Further detailed descriptions of Accusand® properties can be found in (Schroth et al., 1996). The sand was rinsed with DI water 8-10 times, until no turbidity was observed in the supernatant. The rinsed sand was then oven dried at 45° to 50°C for 48 hours, prior to use.

Table 2.1 Accusand® properties, from *Schroth et al. (1996).*

Accusand® grade	12/20	20/30	30/40	40/50
Particle diameter, d_{50} (mm)	1.105	0.713	0.532	0.359
Uniformity coefficient (d_{60}/d_{10})	1.231	1.130	1.207	1.200
Particle density (g/cm^3)	2.665	2.664	2.665	2.663
Porosity	0.348	0.348	0.348	0.348

2.2.2 Solutions

The two infiltrating solutions employed are (A) 5 molal $NaNO_3$ and (B) distilled deionized water (NANOpure® 04751, Barnstead Thermolyne). The physical properties of the solutions are summarized in Table 2.2. Viscosity (Gilmont® low shear falling ball viscometer), density, and surface tension (pendent drop technique on a Kruss® Automated Goniometer DSA 10) were measured for each of the solutions (ThetaDyne Co., Charlotte, NC). The addition of nitrate to the solutions raised the surface tension and viscosity of the solution by promoting the hydrogen bonding strength (Weisbrod et al., submitted a). The molal concentrations represent moles of $NaNO_3$ per kilogram of pure water.

Table 2.2 Solution properties from *Weisbrod et al. (submitted a)*.

Solution	Density (g/cm^3)	Viscosity (cp)	Surface Tension (mN/m)
n-Hexane, pa	0.659	0.314	18.4
5 molal $NaNO_3$	1.247	1.314	80.54
Pure water	0.992	1.001	72.8

2.2.3 Sample Columns

The sand columns were constructed from commercial acrylic tubing with an I.D. of 4.45 cm and an O.D. of 4.76 cm. Three columns were cut on a lathe from a single segment of stock tubing into 25.0 cm lengths for the static experiments. The static columns were fixed with a lower boundary of stainless steel mesh weave #6

(Small Parts Inc., Miami Lakes, FL) cut into circles to fit the bottom of the column. The mesh was attached using a two-part plastic bonding epoxy. In order to prevent the sand grains from sifting through the mesh, a double layer of household cheesecloth was cut into a circular pattern in order to fit the inside of the column and freely rest flat on the stainless steel mesh.

Three additional columns were cut on the lathe into 20.0 cm lengths for the dynamic experiments. The lower boundary of the dynamic columns consisted of a double layer of cheesecloth held taught by epoxy. After the epoxy cured, a layer of silicon was applied onto the overlapping cheesecloth down to the bottom rim of the column. This ensured that the excess cheesecloth would not absorb any liquid during an experiment, which would compromise the imbibition.

2.2.4 Saturated Hydraulic Conductivity

The saturated hydraulic conductivity, K_S, was tested for each grade of sand using the falling head method (Klute and Dirksen, 1986). With a hydraulic head difference H (represented by the head at one point H_1 and the head at a second point H_2) across the sample length x, the volume of water dV that passes through the sample in time dt is given by Darcy's Law

$$\frac{dV}{dt} = -K_S\left(\frac{H}{x}\right) \tag{2.18}$$

We compute dV as adH, where a is the cross-sectional area of the standpipe and dH is the change in ponding height. Integrate between limits t_1, H_1 and t_2, H_2 and solve

for the conductivity K_S to yield the resulting equation for the determining conductivity using the falling head method

$$K_S = \left(\frac{ax}{At}\right)\ln\left(\frac{H_1}{H_2}\right) \tag{2.19}$$

where A is the cross-sectional area of the sample and x is the length or height of the sample. In our experiments $A=a$, since there is no standpipe with a cross-sectional area different than that of the sample. A diagram of the system used for measuring the hydraulic conductivity of the four Accusand® grades is shown in Figure 2.1.

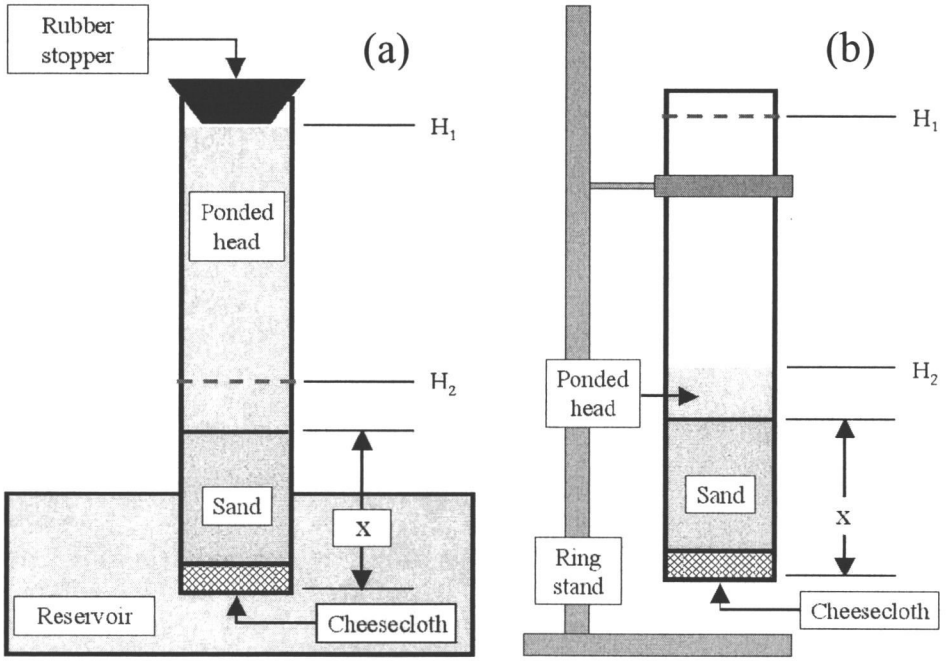

Figure 2.1 Falling head method: The column packed with the sand sample is placed in the reservoir and lowered to fully saturate the media and build a significant ponded head (a). A rubber stopper prevents the column from draining while it is removed from the reservoir and attached to the ring stand (b). To begin the experiment, the stopper is removed to allow drainage into the laboratory sink.

The saturated hydraulic conductivity of each sand grade was determined from the average of three repetitions. The repetitions were conducted using various values for x, H_1, and H_2. The hydraulic resistance of the equipment, consisting of the cheesecloth and the column, was tested without the media, and determined to be negligible, with no measurable effect on the overall calculation of K_S.

2.2.5 Intrinsic Permeability

Referring to the Hagen-Poiseuille equation

$$q = \frac{r^2}{8\mu_l}\frac{dP}{dL} \tag{2.20}$$

it is important to note that we measured pressure in terms of hydraulic head, therefore we make the substitution $\rho_l g h$ for P, to obtain

$$q = \frac{r^2}{8}\frac{\rho_l g}{\mu_l}\frac{dh}{dL} \tag{2.21}$$

The term $r^2/8$ is a geometric term, which is strictly a function of the medium. This can be referred to as the intrinsic permeability, denoted by the symbol κ (Selker et al., 1999). The term $\rho_l g/\mu_l$ is a function of the fluid exclusively, while the term dh/dL is a function of the pressure distribution. We have therefore recovered Darcy's law and have also been able to see why by pulling $\rho_l g/\mu_l$ out of the hydraulic conductivity we obtain an intrinsic property of the solid, which can be applied to a range of fluids (Selker et al., 1999). The saturated hydraulic

conductivity was then determined for each grade of Accusand® based on the intrinsic permeability of the media κ via the following equation

$$\kappa = K_{S\,water}\left(\frac{\mu_{water}}{\rho_{water}}\right) = K_{S_l}\left(\frac{\mu_l}{\rho_l}\right) \tag{2.22}$$

where subscript l denotes either of the other two imbibing solutions (n-hexane or 5 molal $NaNO_3$). Note that the media-specific, geometric term, as well as the pressure term, were dropped out of the equation due to the fact that they do not vary here. The pore structure of the media presumably remains constant. However the fluid, or solution in question, changes.

2.3 EXPERIMENTAL SETUP

2.3.1 Packing the Columns and Porosity

The columns were carefully packed using the packing device shown in Figures 2.2 and 2.3. It utilized a series of screens to randomize the trajectory of the falling sand grains in order to achieve a homogenously packed column. A metal coffee can used to fill the funnel was grounded via the funnel ground in order to reduce static charge which could cause sand grains to attach to the walls of the acrylic columns. Using this system we were able to obtain relatively a consistent porosity, averaging 0.330, across the samples. Table 2.3 shows that the sands were packed to somewhat higher porosities by Schroth et al. (1996) than those used in the current study.

Table 2.3 Porosity for the four grades of Accusand®.

	12/20	20/30	30/40	40/50
[a]Porosity	0.348	0.348	0.348	0.348
[b]Porosity	0.337	0.328	0.330	0.324

[a]From *Schroth et al., 1996*
[b]Average value based on porosity of the packed columns for each sand grade as prepared for the experiments.

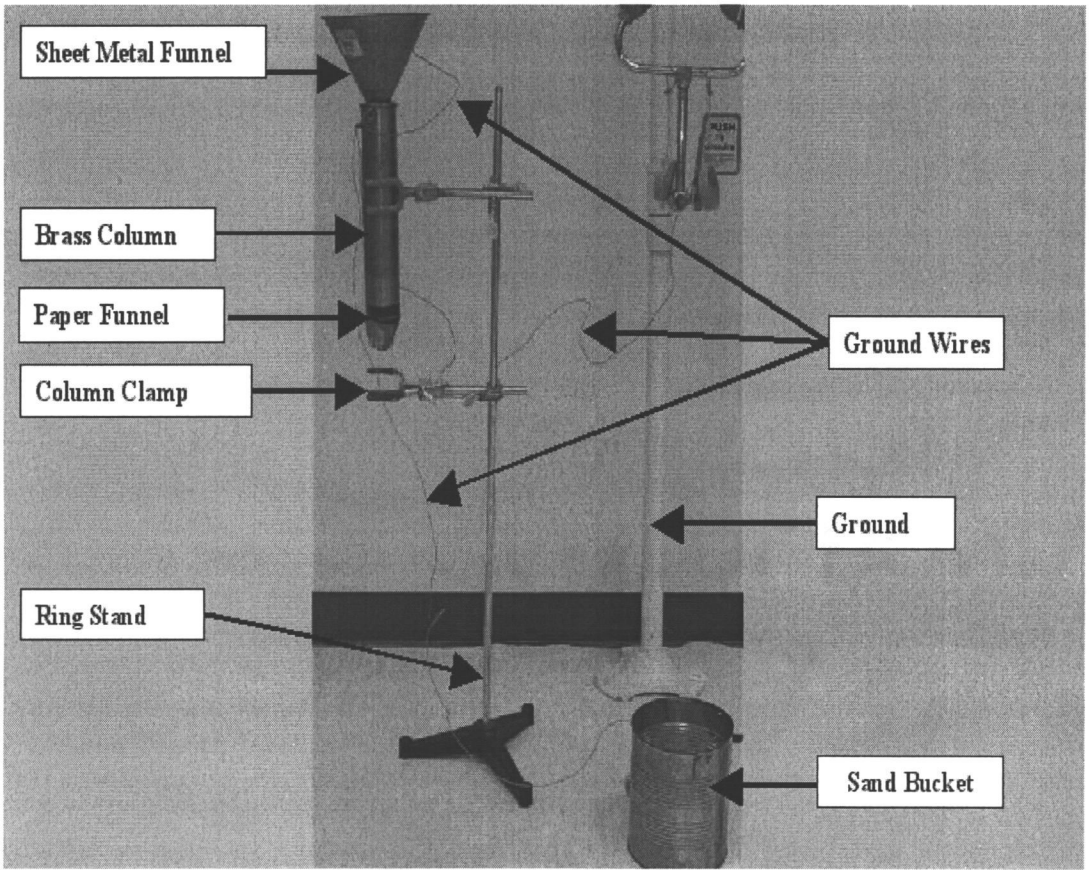

Figure 2.2 Column packing system.

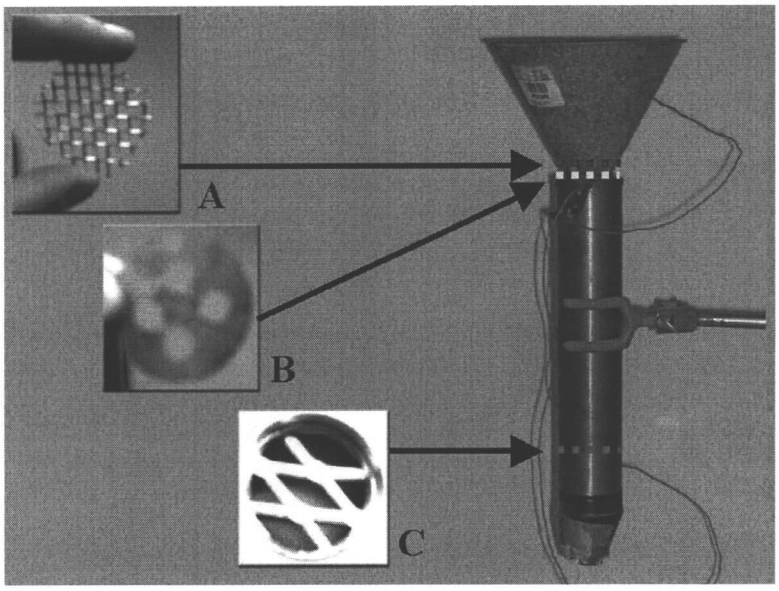

Figure 2.3 Column packing system – Funnel and screen detail.

2.3.2 The Static Method

In the static method experiments, each 25.0 cm column was labeled one through three in order to have three comparable results for each solution tested. Clean cheesecloth was used to line the bottom of each column between each experiment. Each column was packed using the funnel device with the same mass of dry sand achieving relatively uniform porosity between experiments. The filled sand column was then attached to a ring stand and adjusted using a small hand-held leveling device. The liquid, whose wettability was to be tested, was poured into a 1000-ml Pyrex® beaker, placed on a scissor lab jack, and then raised until the surface touched the bottom surface of the sand column. A timer was the set for 24 hours. Clear plastic wrap and Parafilm® were used to cover the mouth of the

beaker and to seal the air space between the top of the beaker and the column to ensure evaporation would not disrupt the samples' contact with the fluid. Furthermore, the tops of the columns were each covered with a 3 in x 3 in corrugated cardboard square to prevent significant evaporation through the media, while still allowing any trapped air to escape during imbibition of the wetting fluid. Particular care was taken in the case of n-hexane due to its volatility. The first repetition for each sand grade used n-hexane to achieve the effective capillary radius r necessary to calculate the contact angle of pure water and 5 molal $NaNO_3$ conducted subsequently. The columns were weighed empty as well as before and after each experiment in order to achieve the mass of liquid imbibed. A total of 12 experiments (3 repetitions for each of three solutions for each of four sand grades) were conducted. The static experimental setup is illustrated in Figures 2.4 and 2.5.

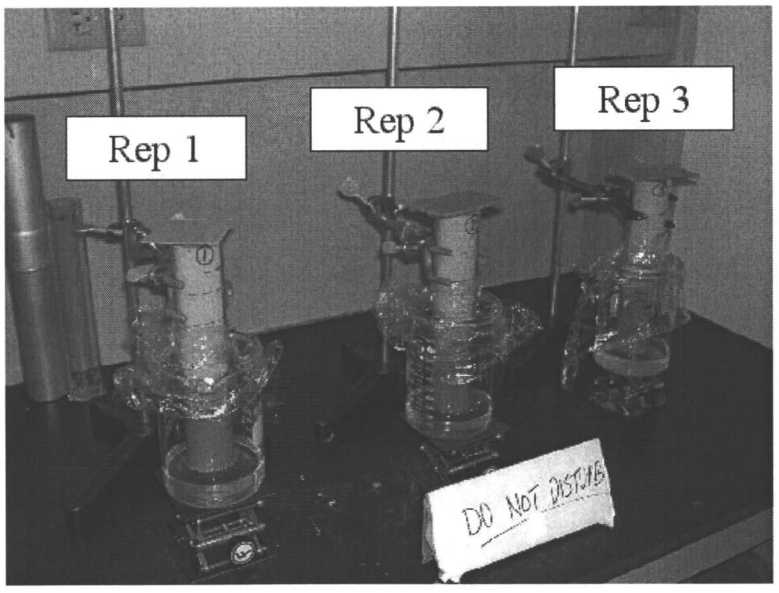

Figure 2.4 Static experiment in progress – three repetitions.

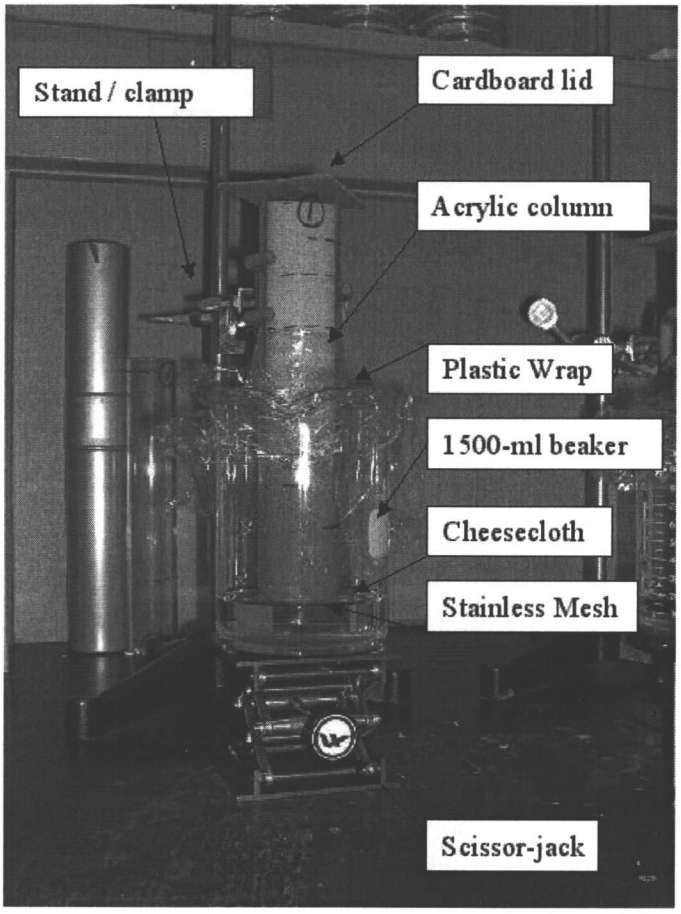

Figure 2.5 Static capillary rise experiment detail.

2.3.3 The Dynamic Method

The second set of experiments utilized the dynamic method. Each 20.0 cm column was labeled one through three. Column one was used for n-hexane, column two for pure water, and column three for 5 molal $NaNO_3$. Three repetitions were conducted for each liquid beginning again with n-hexane. The columns were packed identically with the same mass of sand using the packing funnel to achieve relatively uniform porosity across the samples. A 5.0 kg electronic digital balance

(Setra® Brand) was used to measure the mass of liquid imbibed. The column was attached to the aluminum plate that rested on the balance (Figure 2.7) using a ring stand clamp. The position of the column was adjusted using a hand held leveling device. The balance plate was counter-balanced against the weight of the sand column with an aluminum weight. An 8 in by 6 in Pyrex® baking dish was used as a reservoir for the test liquid. It was placed level on a scissor lab jack and raised until it just touched the bottom of the sand column. Raw data (mass/second) was recorded automatically from the Setra® balance by a Basic language program written using Visual Basic® (see full setup Figure 2.8). The data-logging program was started just prior to touching the liquid to the sand. This program was designed to write the mass per time data to the computer each time the balance stabilized. After the fluid completely imbibed to steady state, the liquid was lowered until the meniscus broke. The data-recording program was then stopped and the raw data was imported to a Microsoft Excel® spreadsheet.

The mass data had to be corrected for surface tension effects before its value was squared. Figure 2.6 illustrates the effect attributed to surface tension forces on the data logged as the experiment progresses. When the column just touches the surface of the fluid, a meniscus immediately forms as the surface tension takes hold of the column. This initial energy exchange causes the balance to register more mass than is actually being drawn into the sand. When the contact is broken between the column and the fluid, the data line drops dramatically. The differences in mass value at this specific point is attributed to the interfacial tension force and

thus subtracted from the mass data before its value is squared. The corrected mass portion was then squared and plotted on the y-axis against the time. The slope of the most linear portion was then deduced and used for the m_l^2/t in Equation 2.9.

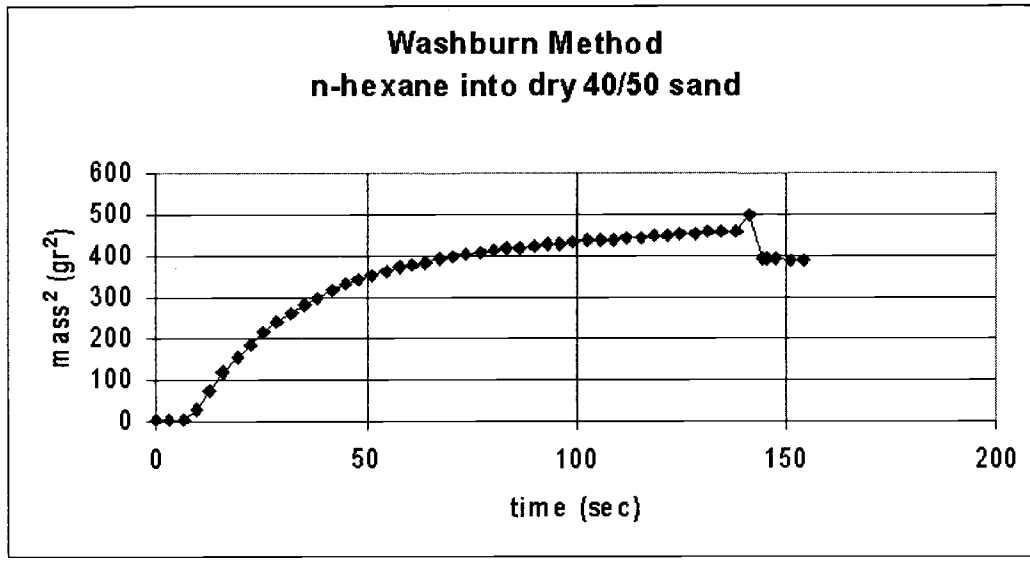

Figure 2.6 Raw data from a dynamic experiment utilizing Washburn's theory. The imbibing fluid is n-hexane into dry 40/50 grade Accusand®. The critical points are (a) where the solution actually begins to imbibe (here at approximately 9 seconds) and (b) when contact between the solution surface and the media is broken at the end of the experiment. The first critical point is compensated for by the modified Green and Ampt model as described in Section 2.3.4. The second critical point represents the surface tension effects which requires the correction to the water mass imbibed (Section 2.3.3).

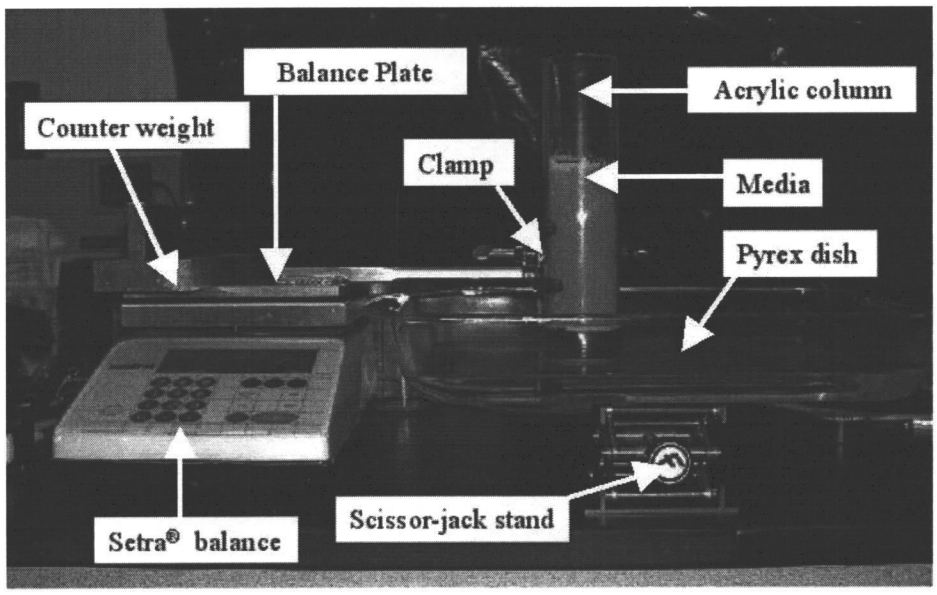

Figure 2.7 Dynamic method experimental assembly detail.

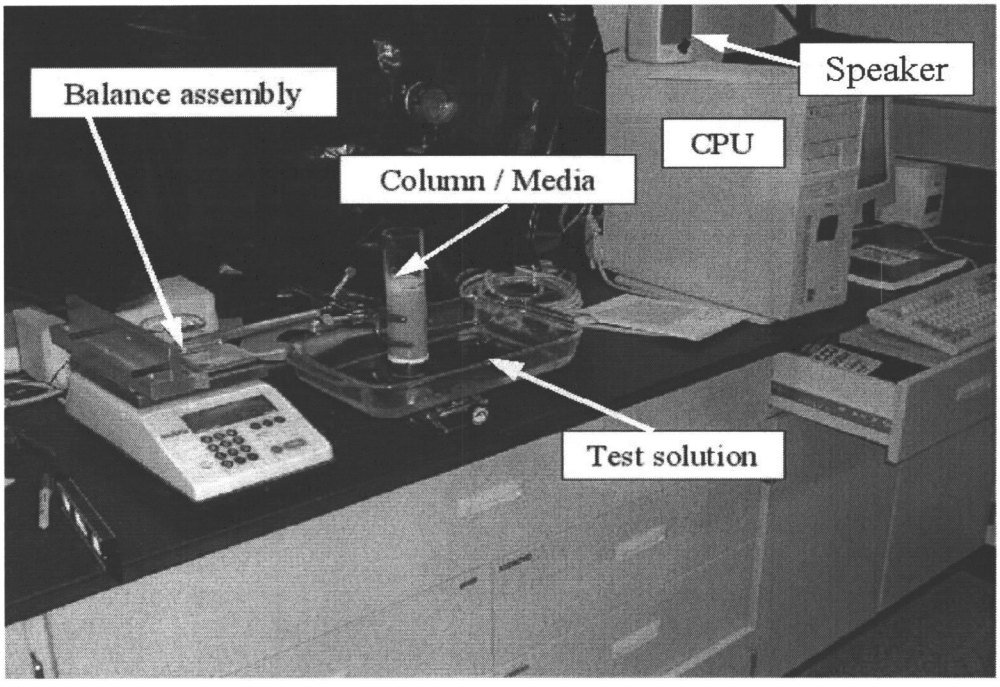

Figure 2.8 Dynamic method experimental setup.

2.3.4 The Analytical Method

The third set of experiments utilized the Green and Ampt solution (Section 2.1.3) to determine the contact angle. Being a dynamic method, the same experimental procedure described in the previous section (Section 2.3.3) was used to obtain the raw data, which is again mass (in grams) per time (in seconds). The mass was corrected for surface tension force affects as described in Section 2.3.3. Time and corrected mass were transferred to a Microsoft Excel® spreadsheet (Figure 2.9). The solver module within Microsoft Excel® was used to minimize the sum of square errors by optimizing t_0, K_{FS}, and h_f. K_{FS} represents the optimized hydraulic conductivity K_S for the revised Green and Ampt model described in Section 2.1.3. The model optimizes a lower hydraulic conductivity than that directly measured (see Table 3.2 and 3.4). Therefore the parameters are assigned different variables to distinguish them from one another. The model was based on a Newtonian method of tangential estimates using forward derivatives, and set to run 100 iterations at a precision of 1×10^{-6} with a 5% error tolerance converging on each point within 1×10^{-4}. The raw data start time was adjusted by subtracting the initial time t_0, optimized by the model, to reflect the actual time elapsed from when fluid actually started to imbibe (noted by the initial increase in sample mass). The model calculated the predicted h value via the following relationship

$$h = \frac{m_l}{\pi r^2 \rho_l \Phi} \tag{2.23}$$

where Φ represents liquid content within the pore space of the media.

The Green and Ampt relationship shown in Equation 2.11, was solved in terms of time t. First solving in terms of dt

$$dt = \frac{\Phi}{K_{FS}}\left(\frac{h}{h_f - h}\right)dh \tag{2.24}$$

Then integrating

$$t = \frac{\Phi}{K_{FS}}\int_0^L \left(\frac{1}{\frac{h_f}{h} - 1}\right)dh \tag{2.25}$$

to get

$$t = \frac{\Phi}{K_{FS}}\left\{-h - h_f\left[\ln\left(h_f - h\right) - \ln\left(h_f\right)\right]\right\} \tag{2.26}$$

Predicted time t is calculated then using the three optimized parameters (t_0, K_{FS}, and h_f) and the predicted capillary pressure potential h (calculated from the mass change) in the following equation

$$t = \frac{\Phi}{K_{FS}}\left\{-h - h_f\left[\ln\left(\frac{h_f - h}{h_f}\right)\right]\right\} \tag{2.27}$$

The value for the effective capillary radius r is calculated via Equation 2.2 when the imbibing fluid is n-hexane into dry Accusand®. The average of three calculated r values from the three repetitions with n-hexane was used along with the known solution parameters to calculate the contact angle of pure water and the 5 molal $NaNO_3$ using Equation 2.6.

Green & Ampt type model applied to upward imbibition				t_0 =	8.84853				
40/50 sand parameters Dry									
Φ [cm^3/cm^3]	0.270			Raw data					
h_f [cm]	7.77			time	adj. time	cor. mass	pred. h	pred. Time	sq. error
K_{FS} [cm/sec]	5.98E-02			0.049					
ρ [g/cm^3]	0.659			3.246					
column radius [cm]	2.2225			6.481					
				9.689	0.84047	5.5	1.991958	1.396813	0.556343
σ	18.4			12.866	4.01747	8.7	3.150915	4.01599	0.00148
m_s	357			16.064	7.21547	11	3.983915	7.228983	0.013513
ρ_s	2.663			19.276	10.42747	12.5	4.527176	10.2073	0.220173
V_T	201.7329			22.476	13.62747	13.7	4.961785	13.29016	0.337309
V_S	134.0593			25.687	16.83847	14.8	5.360177	16.85494	0.016471
γ	0			28.886	20.03747	15.6	5.649916	20.03686	0.000607
r_e	0.007324			32.099	23.25047	16.2	5.867221	22.8458	0.404667
				35.298	26.44947	16.8	6.084525	26.1143	0.33517
θ_S	0.348			38.509	29.66047	17.3	6.265612	29.27915	0.38132
θ_R	0			41.737	32.88847	17.8	6.446699	32.95463	0.066156
K_S	0.139			44.921	36.07247	18.2	6.591569	36.36153	0.289065
λ	6.17			48.136	39.28747	18.5	6.700221	39.25838	0.029087
η	3.32			51.336	42.48747	18.8	6.808873	42.51759	0.030122
K_{FS}	5.98E-02	θ_{fs}	0.270	54.531	45.68247	19.1	6.917526	46.22608	0.543611
				57.744	48.89547	19.3	6.98996	49.00646	0.110993
				60.946	52.09747	19.5	7.062395	52.08907	0.008403
				64.159	55.31047	19.6	7.098613	53.76327	1.547204
								SSE	4.891696

Figure 2.9 Example spreadsheet controlling the Green and Ampt imbibition model used to determine the dynamic contact angle. This particular data set was for a 40/50 grade sand sample using n-hexane as the test fluid in order to calculate r. Note the contact angle γ set at the assumed value zero.

Brooks and Corey (1964) presented an analytical solution for determining the degree of saturated hydraulic conductivity at any given water content expressed as

$$K(\theta) = K_S\left(\frac{\theta - \theta_0}{\theta_S - \theta_0}\right)^{\eta} \quad \text{for } h < h_f \tag{2.28}$$

where $\eta = \frac{2}{\lambda} + 3$.

$K(\theta)$ represents conductivity at a given degree of saturation θ, K_S is the measured saturated hydraulic conductivity of the soil, θ_0 is the residual saturation of the soil, θ_S is the full saturation of the soil, and λ is the fitting parameter for the media. Equation 2.28 may be solved in terms of θ.

$$\theta = \left[(\theta_S - \theta_0) \left(\frac{K(\theta)}{K_S} \right)^{\frac{1}{\eta}} \right] + \theta_0 \tag{2.29}$$

Because K_{FS} represents the hydraulic conductivity at some degree of water content, the $K(\theta)$ term from the Brooks and Corey solution represents K_{FS} determined by the modified Green and Ampt model. Full saturation θ_S is taken from Table 2.4. Residual saturation θ_0 and the fitting parameter λ were taken from Schroth et al. (1996). Residual saturation θ_0 was set at zero to reflect the initially dry sand experiments. The degree of saturation θ is called θ_{fs} here as it is related to the fitting parameter K_{FS}. The model calculates θ_{fs} via Equation 2.29 based on the fitted K_{FS} achieved during optimization. The Φ parameter is changed to the same value as the calculated degree of saturation θ_{fs} term. The model is run again until the two terms (θ_{fs} and Φ) converge, providing the final solutions for K_{FS}, h_f, and t_0.

2.3.5 Falling Head Method for Saturated Hydraulic Conductivity

The falling head experiments for determining saturated hydraulic conductivity were conducted in the following manner. The acrylic columns were fitted with a

lower boundary of double layered cheesecloth secured tightly with a thick rubber band and packed using the same method described earlier to various heights. Tick marks were placed at 1.0 cm intervals on the sides of the columns. A large bucket was filled with NANOpure® filtered water and the packed columns were submerged and held in the bucket for 10 minutes to saturate the media. A specially constructed apparatus called the plunger was used to hold the media in place while allowing the water and air to flow from the lower boundary up through the surface boundary of the sample (Figure 2.10). In previous trials, the media would float and separate unless it was held in place when saturated under positive pressure.

After 10 minutes, the plunger was slowly removed to avoid disturbing the sample and the column was slowly raised above the water line, keeping the media submerged while maintaining an arbitrary height of ponded head in the column. While in this position, the top of the column was fitted with a rubber stopper to hold the ponded head. Then the column in its entirety was pulled from the bucket. The height of the sample x and the height of the ponded head, H_1, were both noted (Figure 2.1a). The column was fixed to a ring stand over the laboratory sink and checked with a hand level. At the same time the stopper was removed, a stop watch was started and stopped at a predetermined point, H_2, which was lower on the column below H_1, but before the ponded head reached the surface of the sand (Figure 2.1b).

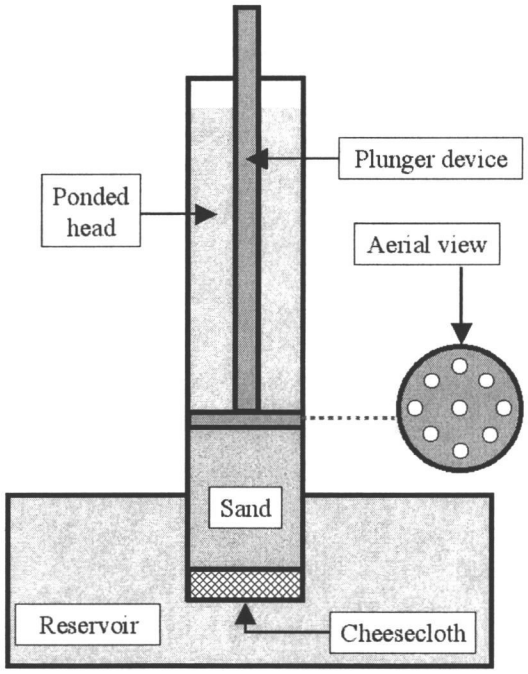

Figure 2.10 Plunger device used to hold sand in place. An aerial view to illustrate air holes, through which trapped air within the system can escape.

2.3.6 Pre-wetted Sand

The experiments using the pre-wetted sand were prepared in the same manner as the dry sand experiments just before saturation. Three columns were packed with the same grade of sand to obtain the three repetitions needed for comparison to the dry sand experiments. They were then bound together with a rubber band to ensure stability and placed upright on top of a stainless steel mesh grating in a large bucket. The bucket was slowly filled with NANOpure® water within 3.0 cm of the top of the columns. The columns were allowed to sit for 2 hours to ensure complete saturation and force as much trapped air as possible from the pore space. The columns were then removed from the water bath and reweighed on the balance.

A Soil Moisture Equipment Company (Santa Barbara, CA - Catalog # 1500) 15-bar ceramic plate Extractor, which we call a pressure bomb (Figure 2.11), was fitted with a 1 bar pressure porous ceramic plate (Figure 2.12) was used to force the saturated columns to residual water content. The pressure plate was soaked thoroughly overnight, then placed in the pressure bomb and hooked up to the outflow tube. A thin layer of 40/50 sand was spread over the surface of the plate and then the columns placed directly on the sand upright. This interim layer ensured a continuous hydraulic connection with the sample. Damp cheesecloth was draped over the top of the columns with the corner placed in a beaker of water (left in the pressure bomb) in order to keep the cloth damp. This was done to prevent any evaporation from the top portion of the sample within the columns (Figures 2.13 and 2.14).

The pressure bomb was sealed and set for pressure of 3.0 psi, equivalent to 0.21 bar or 210 cm of water. This exceeds the air entry pressure head of all the sand grades by at least a factor of four (Schroth et al., 1996). The columns were placed under this constant pressure for 12 hours, then removed from the pressure bomb and reweighed.

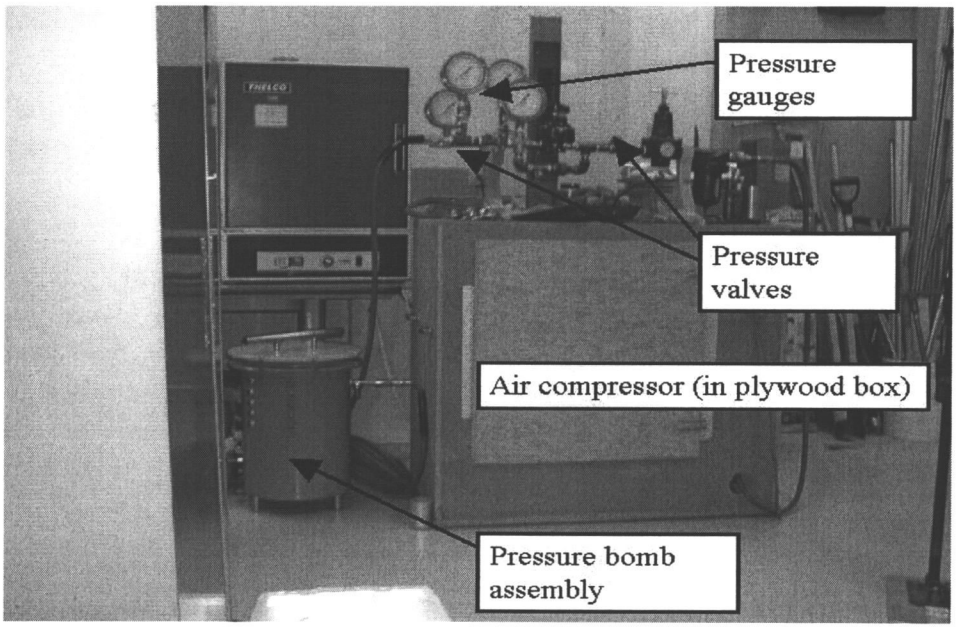

Figure 2.11 Pressure bomb assembly with control valves and air compressor generator.

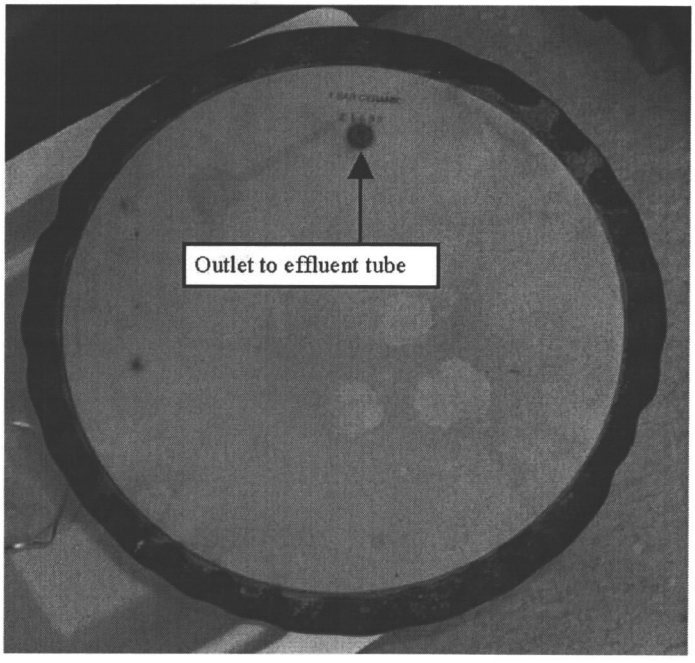

Figure 2.12 1 bar porous pressure plate used to extract resident water from the sand columns.

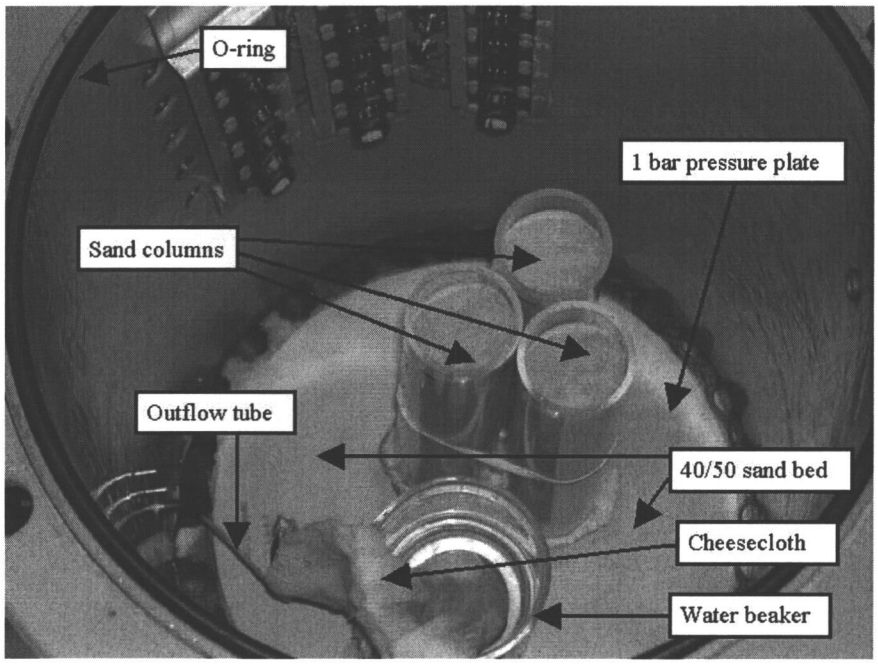

Figure 2.13 Pressure bomb detail – sand columns uncovered

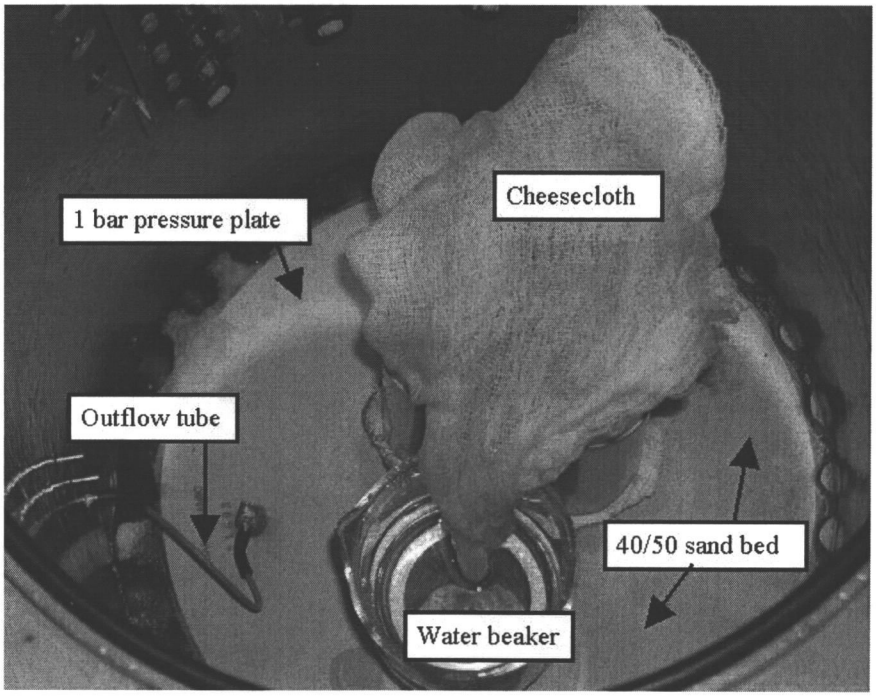

Figure 2.14 Pressure bomb detail – sand columns covered

To assess the conditions achieved in this method, three additional columns were marked in ten segments of 2.5 cm each (with segment one at the top boundary and segment ten at the lower boundary) to gravimetrically determine water content. Each of these segments was extracted, then placed in a petri dish and weighed. The samples were then oven dried at 45° to 50°C for 24 hours after which, they were reweighed (Figure 2.15). These three sample columns (divided into ten samples each) were used to determine the residual water content distribution in the sand sample achieved by the pressure bomb during the prescribed time period. The three columns used for the actual experiment were allowed to imbibe the test solution for 24 hours. The tops of these three columns were covered as in the dry static experiments, with a 3 in x 3 in corrugated cardboard square to prevent significant evaporation while still allowing any trapped air to escape during imbibition of the wetting fluid.

Pre-wetted sample columns for the dynamic method experiments were prepared in the same manner using the pressure bomb, however no gravimetric sampling was conducted. The analytical model was run using the raw data generated, with the residual saturation θ_R values given in Table 4.2 included in the calculations using Equation 2.31.

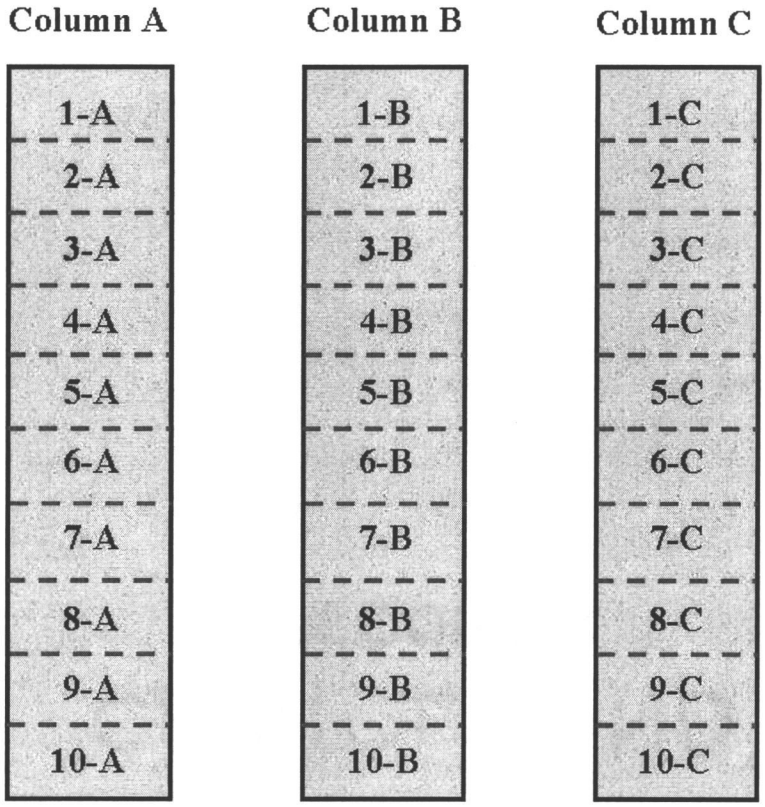

Figure 2.15 Gravimetric sample configuration for pre-wetted sand columns utilizing the static method.

3 RESULTS

3.1 HYDRAULIC CONDUCTIVITY

Results from the falling head method for measuring the saturated hydraulic conductivity K_S of the four Accusand® grades are summarized in Table 3.1. Each value of K_S is the mean of three repetitions with standard deviations shown in parentheses. The K_S values from Schroth et al. (1996) for the same grades of Accusand® are included for comparison. Measurements of saturated hydraulic conductivity by Schroth et al. (1996) were performed during upward flow using the constant-head method (Klute and Dirksen, 1986). As previously noted, porosity values for packed samples were 1 % to 2 % lower (Table 2.4) than those achieved by Schroth et al. (1996), thus the lower K_S values are to be expected.

Table 3.1 Laboratory measured K_S of four sand grades using pure water.

	40/50	30/40	20/30	12/20
[a]K_S (cm/sec)	0.065 (0.002)	0.115 (0.002)	0.228 (0.009)	0.476 (0.016)
[b]K_S (cm/sec)	0.072	0.149	0.250	0.503

[a]As measured via falling head method (Section 2.2.4).
[b]From *Schroth et al., 1996.*

Equation 2.24 was used to calculate the K_S for the various sand grades for the different the test fluids that have different densities and viscosities than pure water based on the intrinsic permeability of the media (see Section 2.2.5).

Table 3.2 Calculated K_S of four sand grades using test solutions.

	40/50	30/40	20/30	12/20
	K_S (cm/sec)	K_S (cm/sec)	K_S (cm/sec)	K_S (cm/sec)
n-hexane	[b]0.139	[b]0.247	[b]0.489	[b]1.021
Water	[a]0.065	[a]0.115	[a]0.228	[a]0.476
5 m $NaNO_3$	[b]0.062	[b]0.110	[b]0.218	[b]0.456

[a]As measured via the falling head method and reported in Table 3.1.
[b]As calculated using the intrinsic permeability (Section 2.2.5).

3.2 DRY SAND

3.2.1 Static Method

The results from the applied static method in initially dry sands are summarized in Table 3.3. The figures are mean contact angles obtained from three repetitions conducted with each of the two test solutions (water and 5 molal $NaNO_3$) imbibing each of the four sand grades. Figure 3.1 summarizes the discrete points representing the mean contact angle for each fluid imbibing each sand grade with error bars representing the standard deviation. Figure 3.2 is provided to illustrate the comparison of contact angles across all sand grades between the two solutions. Standard deviations are provided in parentheses.

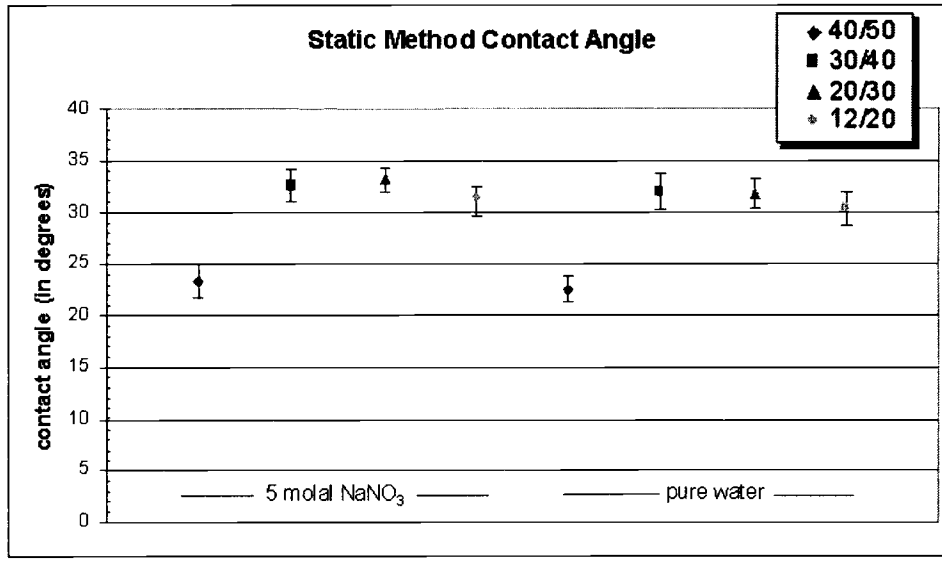

Figure 3.1 The following discrete data points represent the mean contact angle measurement between three repetitions for both solutions with each sand grade. Error bars show the standard deviation between repetitions.

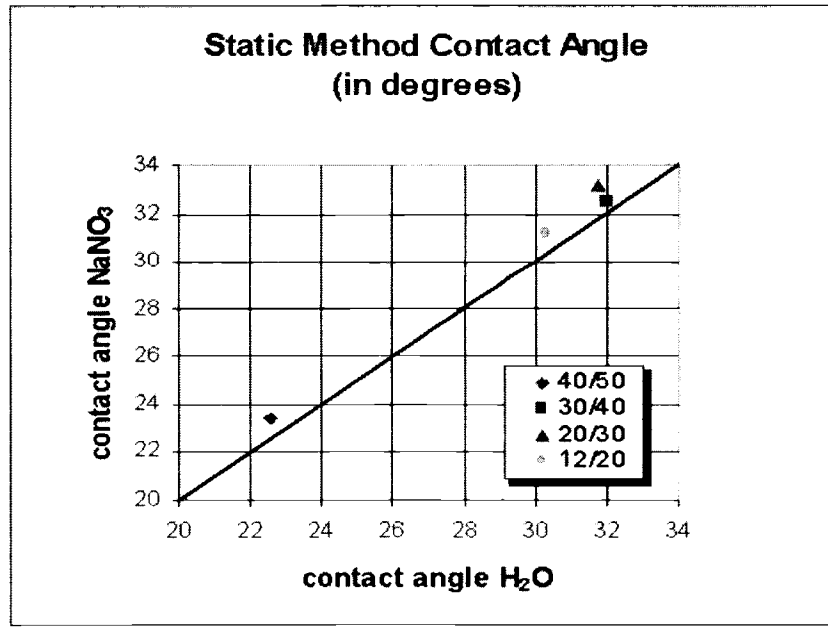

Figure 3.2 This graph illustrates the similarity in contact angle measurements between the water and the salt solution into dry sand.

Table 3.3 Static Method Results, Dry Sand.

Sand	Solution	[a]Capillary rise, h (in cm)	[b]Pore radius, r (in cm)	[c]Contact angle (in degrees)
40/50	n-hexane	6.68 (0.10)	0.009 (0.0001)	0
	Pure water	16.20 (0.25)	0.009 (0.0001)	23 (1.15)
	5 m $NaNO_3$	14.17 (0.03)	0.009 (0.0001)	23 (1.71)
30/40	n-hexane	5.15 (0.10)	0.011 (0.0002)	0
	Pure water	11.48 (0.19)	0.011 (0.0002)	32 (1.71)
	5 m $NaNO_3$	10.04 (0.01)	0.011 (0.0002)	33 (1.59)
20/30	n-hexane	3.68 (0.07)	0.016 (0.0003)	0
	Pure water	8.22 (0.03)	0.016 (0.0003)	32 (1.37)
	5 m $NaNO_3$	7.13 (0.04)	0.016 (0.0003)	33 (1.22)
12/20	n-hexane	2.52 (0.09)	0.023 (0.0008)	0
	Pure water	5.72 (0.10)	0.023 (0.0008)	30 (1.65)
	5 m $NaNO_3$	4.99 (0.11)	0.023 (0.0008)	31 (1.26)

[a]Height of capillary rise calculated via Equation 1.8.
[b]Effective pore radius representing the sand calculated via Equation 1.9.
[c]Advancing contact angle of the solution on the sand calculated via Equation 1.10.

3.2.2 Dynamic Method

The results from the dynamic method (Table 3.4) include only those using the analytical solution. The data from the dynamic experiments did not satisfy the assumed square root of time behavior in Washburn's theory, so it could not be interpreted in this manner. This point is further discussed in Section 4.3. Figures 3.3 through 3.14 illustrate the model's ability to fit the raw imbibtion data adjusted for the three test solutions (Table 2.2) into each sand grade (Table 2.1). Each graph represents one repetition using each solution for each sand grade.

Table 3.4 Dynamic Method Results, Dry Sand.

Sand / Solution	[a]Pressure potential, h_f (cm)	[b]Pore radius, r (cm)	[c]K_{FS} (cm /sec)	[d]Contact angle (degrees)	[e]Water content, θ_{fs}
40/50					
n-hexane	7.71 (0.09)	0.007 (0.000)	0.058 (0.002)	0	0.267 (0.002)
Pure water	13.27 (0.95)	0.007 (0.000)	0.043 (0.004)	49 (3.54)	0.308 (0.009)
5 m $NaNO_3$	13.38 (0.55)	0.007 (0.000)	0.031 (0.002)	41 (2.70)	0.282 (0.006)
30/40					
n-hexane	6.55 (0.42)	0.009 (0.001)	0.068 (0.006)	0	0.235 (0.005)
Pure water	8.62 (0.04)	0.009 (0.001)	0.071 (0.002)	60 (0.14)	0.301 (0.003)
5 m $NaNO_3$	9.36 (0.67)	0.009 (0.001)	0.047 (0.004)	52 (3.24)	0.269 (0.008)
20/30					
n-hexane	6.01 (0.25)	0.010 (0.000)	0.063 (0.007)	0	0.189 (0.006)
Pure water	6.43 (0.56)	0.010 (0.000)	0.107 (0.015)	66 (2.23)	0.278 (0.001)
5 m $NaNO_3$	6.41 (0.39)	0.010 (0.000)	0.074 (0.007)	63 (1.79)	0.252 (0.007)
12/20					
n-hexane	4.85 (0.39)	0.012 (0.001)	0.049 (0.006)	0	0.147 (0.005)
Pure water	5.52 (0.49)	0.012 (0.001)	0.102 (0.032)	64 (2.44)	0.223 (0.006)
5 m $NaNO_3$	4.57 (0.44)	0.012 (0.001)	0.116 (0.037)	66 (2.44)	0.222 (0.001)

All values are based on the mean of three repetitions per solution for each grade of Accusand®. Standard deviations are provided in parentheses.
[a]Capillary pressure potential fitted by the Green and Ampt model.
[b]Effective pore radius calculated via Equation 2.4 using the solution specific parameters (σ_{lg} and ρ_l) for n-hexane, as well as that optimized by the modified Green and Ampt model (h_f) while assuming γ to be zero for n-hexane.
[c]K_{FS} fitted by the Green and Ampt model.
[d]Advancing contact angle of the solution on the sand rise calculated via Equation 1.10 using fitted parameters, except for n-hexane for which a contact angle of zero was assumed.

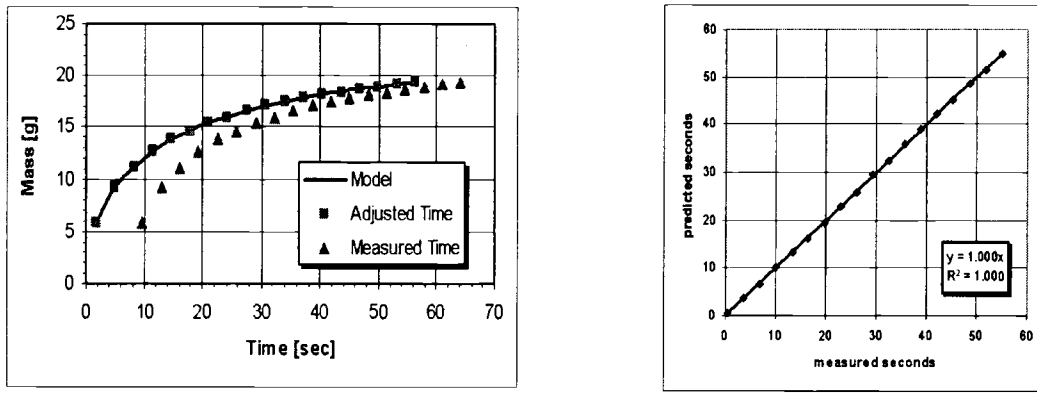

Figure 3.3 N-hexane imbibing into 40/50 grade sand.

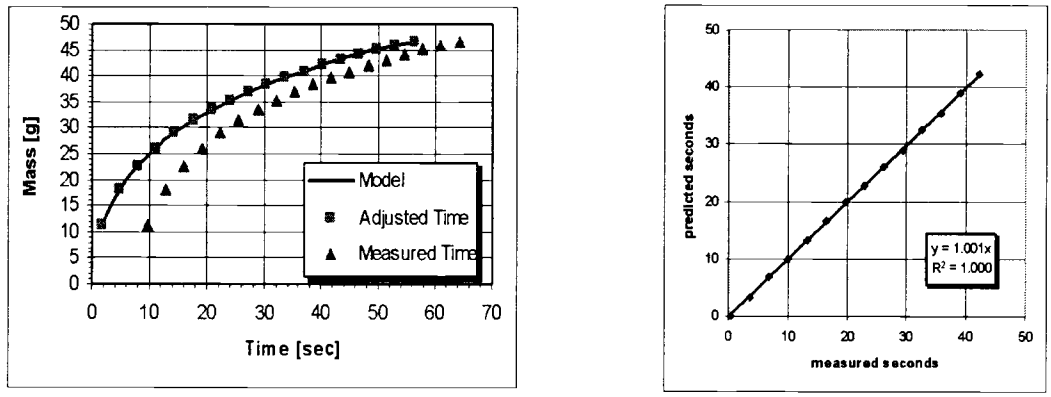

Figure 3.4 Pure water imbibing into 40/50 grade sand.

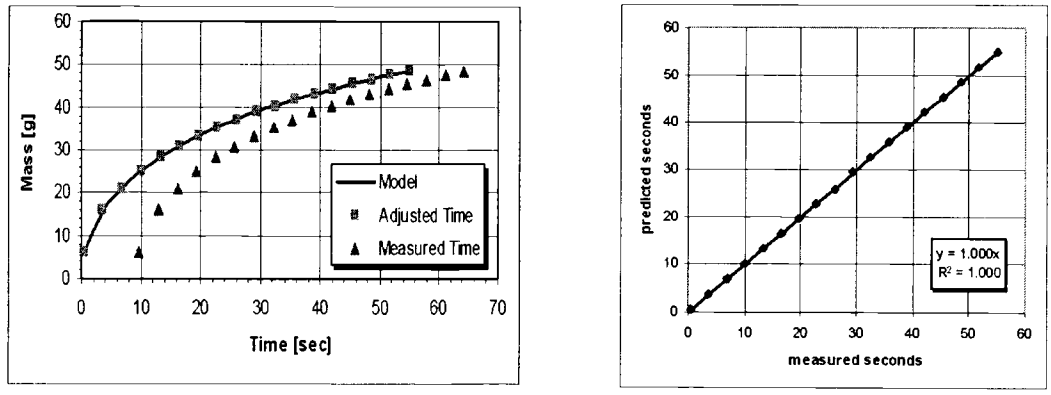

Figure 3.5 5 molal $NaNO_3$ solution imbibing into 40/50 grade sand.

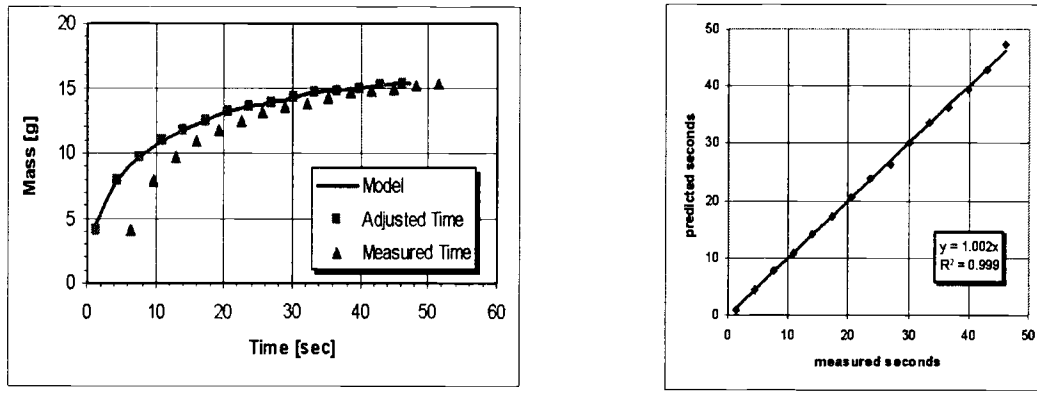

Figure 3.6 N-hexane imbibing into 30/40 grade sand.

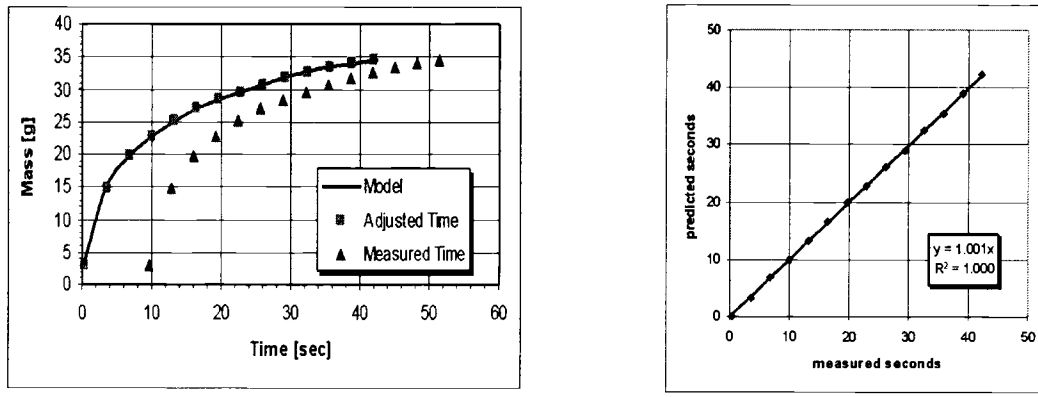

Figure 3.7 Pure water imbibing into 30/40 grade sand.

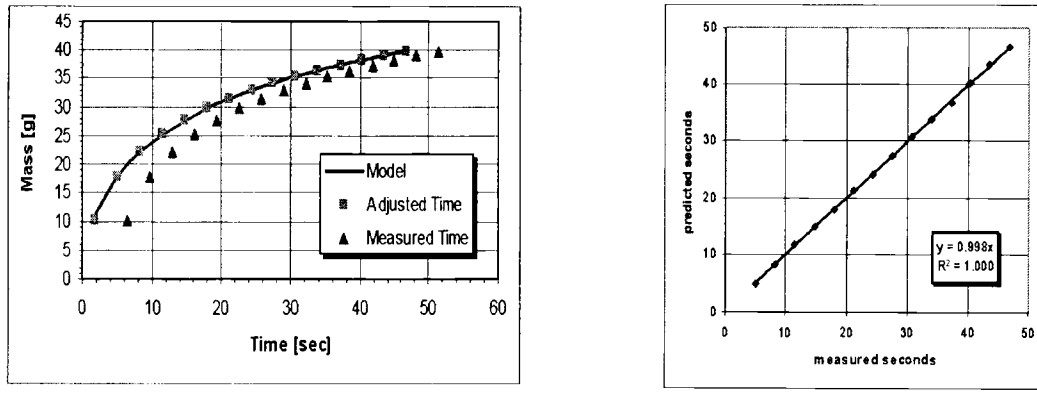

Figure 3.8 5 molal $NaNO_3$ solution imbibing into 30/40 grade sand.

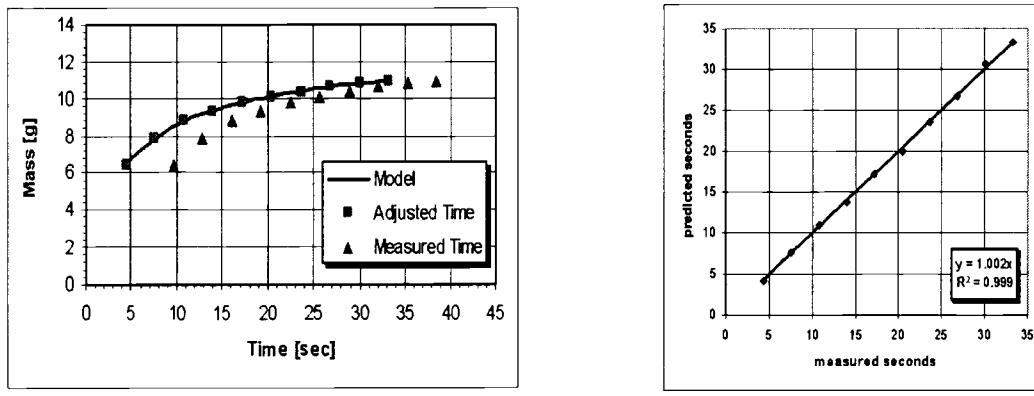

Figure 3.9 N-hexane imbibing into 20/30 grade sand.

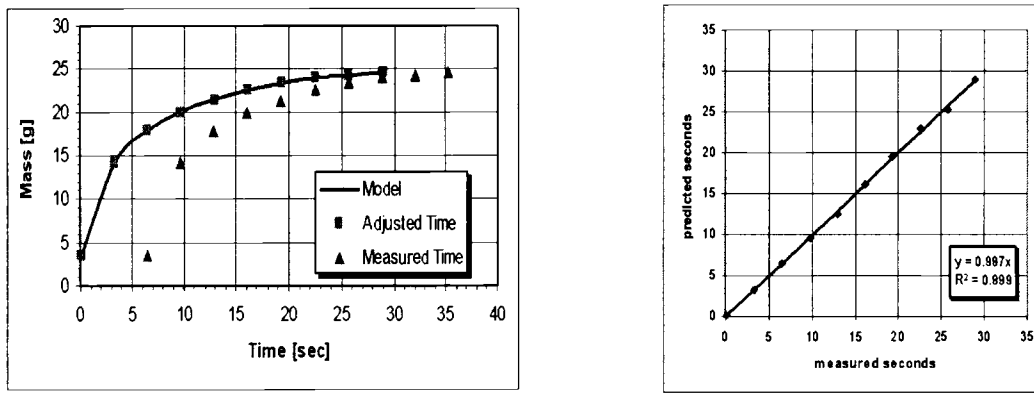

Figure 3.10 Pure water imbibing into 20/30 grade sand.

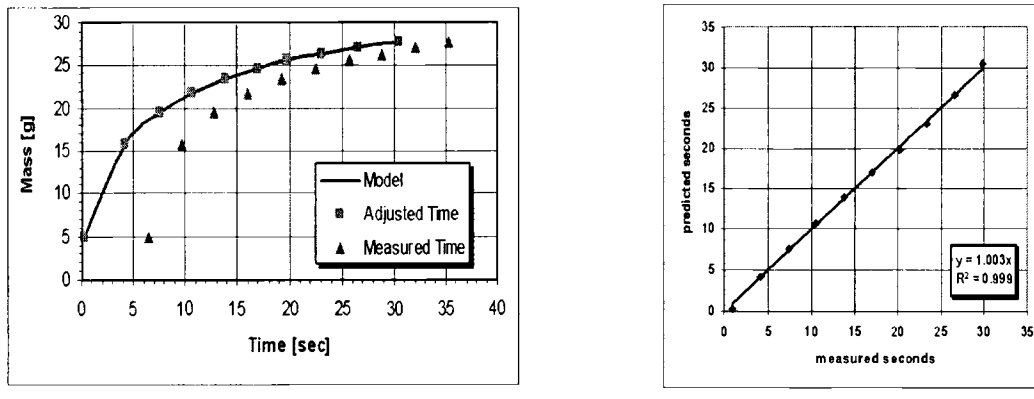

Figure 3.11 5 molal $NaNO_3$ solution imbibing into 20/30 grade sand.

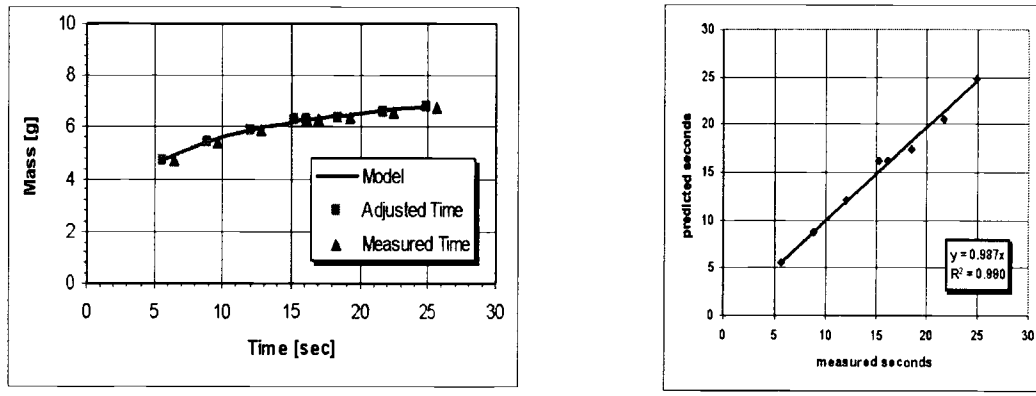

Figure 3.12 N-hexane imbibing into 12/20 grade sand.

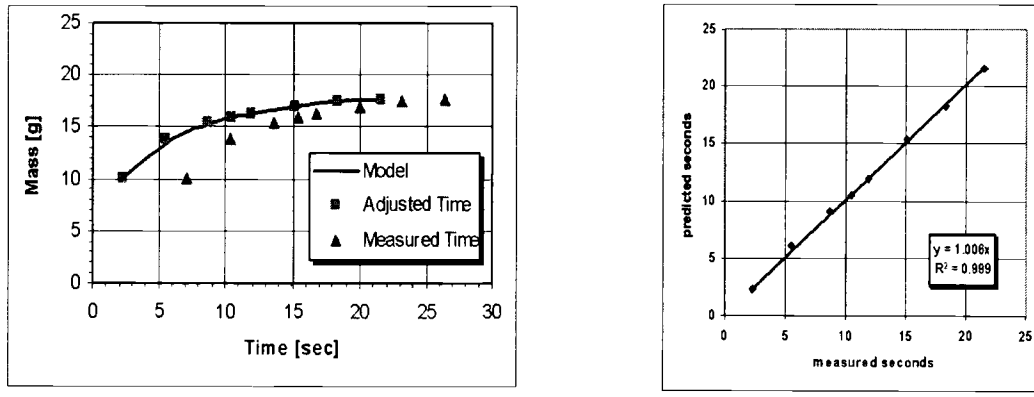

Figure 3.13 Pure water imbibing into 12/20 grade sand.

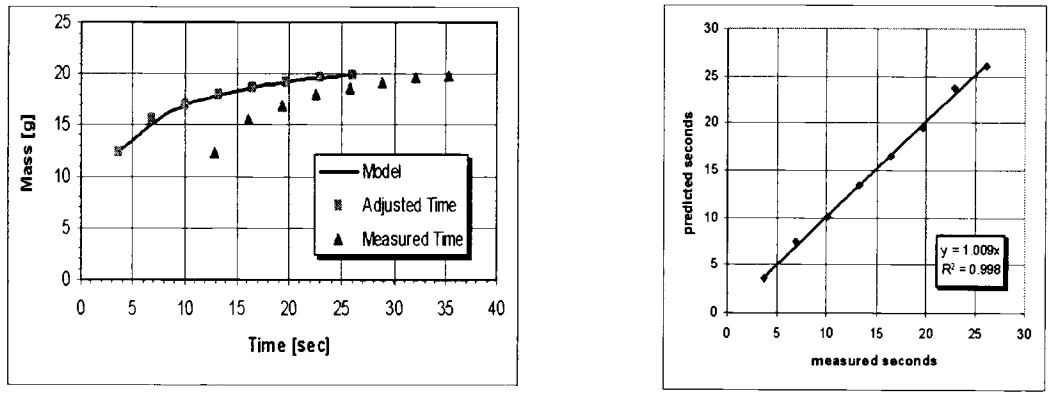

Figure 3.14 5 molal $NaNO_3$ solution imbibing into 12/20 grade sand.

One can see that that the model fits the experimental data exceptionally well, and the fitted line between predicted time and actual measured time has a slope within 1% of unity in all cases with an r-squared of 0.99 or greater.

3.3 PRE-WETTED SAND

3.3.1 Water Content

The results of the gravimetric sampling experiments addressed in Section 2.3.6, are summarized in Figure 3.15. The volumetric water content θ_v of each segment in the column prior to the imbibition experiments was calculated in the following manner:

$$w = \frac{M_w}{M_s} \tag{3.1}$$

where M_w is the mass of water in the sample in grams, which is determined after oven drying the sample, and M_s is the dry mass of the sand (in grams) of each sample. Therefore w represents the gravimetric (or mass basis) water content in grams per gram.

The volumetric water content θ_v is calculated by taking the gravimetric water content w and multiplying by the bulk density of the sample ρ_b over the density of the water ρ_w, taken here to be simply one.

$$\theta_v = w\left(\frac{\rho_b}{\rho_w}\right) \tag{3.2}$$

The dry bulk density of the sand ρ_b was taken to be

$$\rho_b = \frac{M_S}{V_T} \tag{3.3}$$

where V_T is the total volume occupied by the sample. Dry bulk density ρ_b values were calculated based on the entire column. Each of the ten segments in each of the three columns were assigned the ρ_b calculated for that particular column. This was done for simplicity since the gravimetric sampling was somewhat destructive. Table 3.5 provides dry bulk density for each column, which correspond to the segmented samples graphically represented in Figure 3.17 respectively.

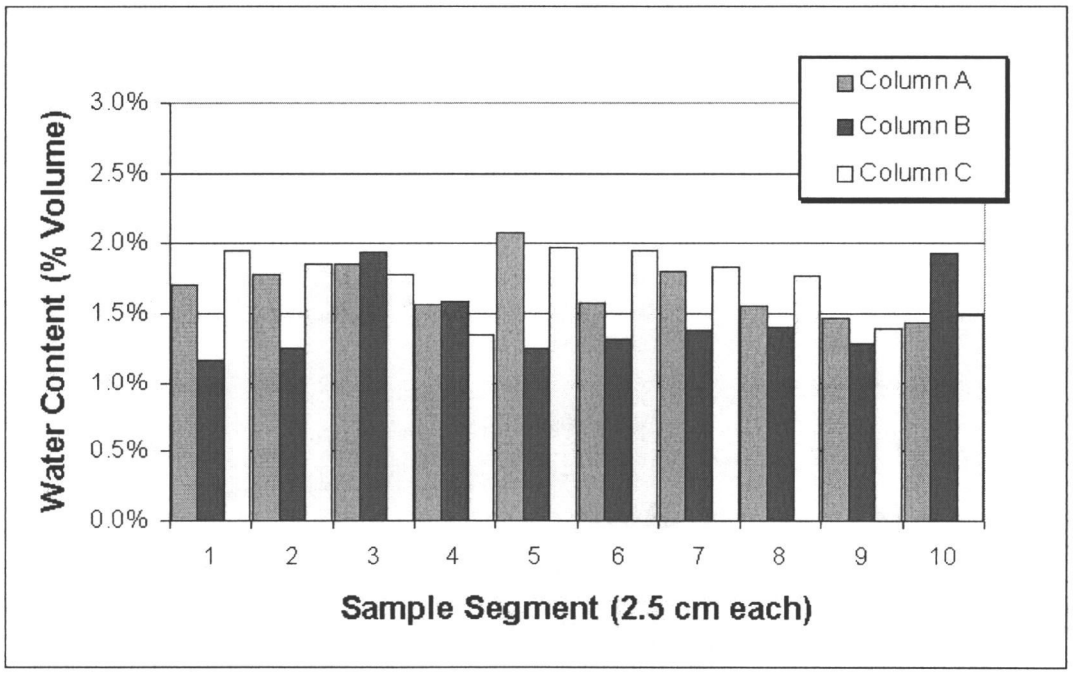

Figure 3.15 Residual water content of three sample columns (A, B, and C) of 40/50 grade Accusand®.

Table 3.5 Dry bulk density ρ_b for gravimetric samples.

Sample	Column A	Column B	Column C
[a]M_S (g)	686.7	687.5	688.8
[b]V_T(cm^3)	387.1	387.1	387.1
[c]ρ_b (g/cm^3)	1.77	1.78	1.78

[a]Total dry mass of sand in each column.
[b]Total volume of each column occupied by the sand.
[c]Dry bulk density of each column.

The volumetric water content θ_v in cm^3/cm^3 was then converted to percent saturation as shown in Figure 3.15. This figure represents one set of three sample columns similarly packed, saturated, and placed in the pressure bomb for 12 hours (Section 2.3.6). Residual saturation of the 40/50 grade Accusand® was found to be approximately 2% in previous work (Schroth et al., 1996 and Weisbrod et al., submitted a), while values obtained in this work ranged from 1.2% to 2.05% with a mean of 1.62% volumetric.

3.3.2 Static Method

The results from the static method in pre-wetted 40/50 grade Accusand® are summarized in Table 3.6. The table reports the mean values between three repetitions conducted with each of the two test solutions (water and 5 molal $NaNO_3$) into each of the four sand grades. Each contact angle measurement

represents the mean contact angle for each fluid on the 40/50 grade sand with standard deviations shown in parentheses.

Table 3.6 Static Method Results, pre-wetted 40/50 sand.

Solution	[a]Capillary rise, h (in cm)	[b]Pore radius, r (in mm)	[c]Contact angle (in degrees)
Pure water	12.50 (0.16)	0.009 (0.0001)	45 (1.01)
5 m $NaNO_3$	10.81 (0.13)	0.009 (0.0001)	46 (1.35)

[a]Height of capillary rise calculated via Equation 1.8.
[b]Effective pore radius representing the sand calculated via Equation 1.9.
[c]Advancing contact angle of the solution on the sand calculated via Equation 1.10.

These results are interesting in that the calculated contact angle is actually greater for both solutions than the contact angles calculated using the static method with initially dry sand (Table 3.3).

3.3.3 Dynamic Method

The results from the dynamic method (Table 3.7) below include only those using the analytical solution since the data did not conform to the assumptions of the standard Washburn model (see Section 4.3 of the Discussion).

Table 3.7 Dynamic Method Results, pre-wetted 40/50 sand. Each value represents three replications, with the standard deviation indicated in parenthesis.

Solution	[a]Pressure potential, h_f (cm)	[b]Pore radius, r (cm)	[c]K_{FS} (cm /sec)	[d]Contact angle (degrees)	[e]Water content, θ_{fs}
Pure water	20.27 (0.02)	0.007 (0.000)	0.006 (0.001)	2 (0.96)	0.141 (0.007)
5 m $NaNO_3$	16.62 (0.13)	0.007 (0.000)	0.006 (0.002)	21 (1.10)	0.141 (0.020)

[a]Capillary pressure potential fitted by the Green and Ampt model.
[b]Effective pore radius calculated via Equation 2.4 using the solution specific parameters (σ_{lg} and ρ_l) for n-hexane, as well as that optimized by the modified Green and Ampt model (h_f) while assuming γ to be zero for n-hexane (dry imbibition only, from Table 3.4).
[c]K_{FS} fitted by the Green and Ampt model.
[d]Advancing contact angle of the solution on the sand rise calculated via Equation 1.10 using fitted parameters.

Again, the model fit the data exceptionally well, with the fitted line between predicted time and actual measured time having a slope within 1% of unity in all cases with an r-squared of 0.99 or greater (Figures 3.16, 3.17 and 3.18).

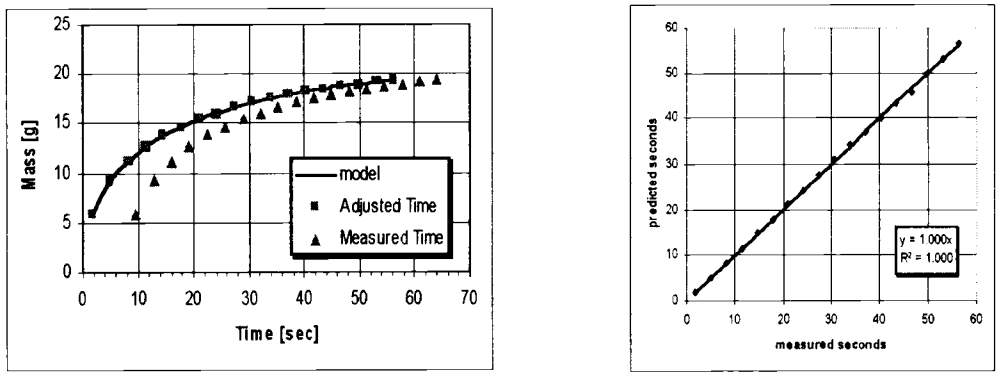

Figure 3.16 N-hexane imbibing into pre-wetted 40/50 grade sand.

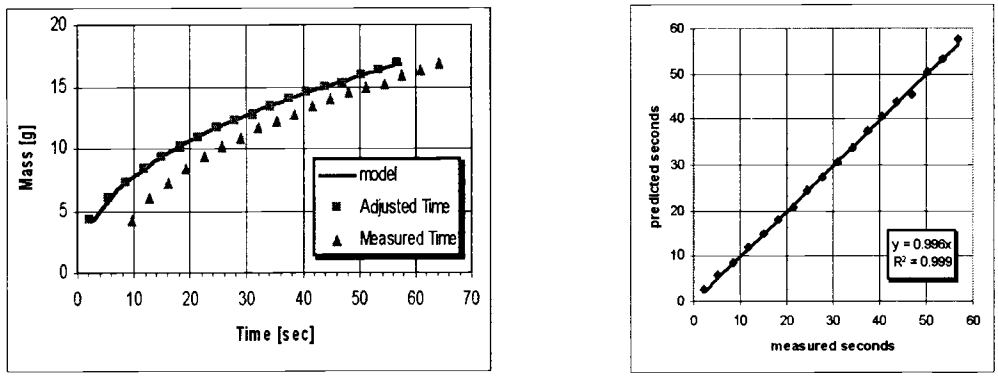

Figure 3.17 Pure water imbibing into pre-wetted 40/50 grade sand.

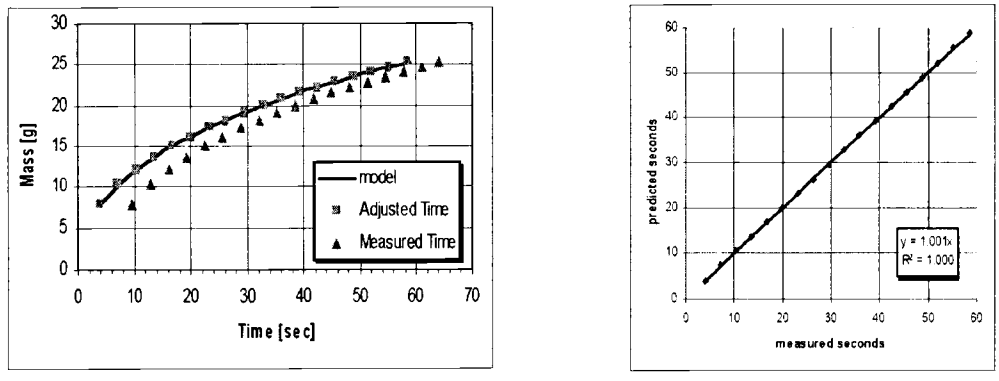

Figure 3.18 5 molal $NaNO_3$ imbibing into pre-wetted 40/50 grade sand.

4 DISCUSSION

4.1 OVERVIEW

The experimentally obtained conductivity parameters (K_S and K_{FS}) were converted to intrinsic permeabilities (κ_S and κ_{FS}) in order to isolate the effects of the media from the various fluids used for imbibition. We then make a comparison between the dynamic solutions showing that gravity cannot be neglected in coarse porous media such as sand, therefore the standard dynamic solution employing Washburn's theory could not be applied. Further, the falling head values of K_S were used in the revised Green and Ampt imbibition model to illustrate that the media did not achieve full saturation at the wetting front. This hypothesis was corroborated using the Brooks and Corey conductivity model, for given conductivities K_{FS} fitted by the analytical model for each grade of Accusand®. It is shown that the effective pore space occupied by resident water, and that which is filled during imbibition, are critical to the determination of the wetting front potential, and ultimately, the contact angle.

4.2 INTRINSIC PERMEABILITY

Table 4.1 below summarizes the results presented in the previous chapter (Tables 3.1, 3.2 and 3.4) from the falling head experiments conducted on the four grades of Accusand®. The measured saturated hydraulic conductivity K_S of the

sands with water was shown to have good reproducibility in Section 3.1 and the K_S values are similar to the values reported by Schroth et al. (1996) using the same silica sands. It is useful to consider the intrinsic permeabilities in order isolate the effects of the media exclusively. It is interesting to look at the ratio of the values for the intrinsic permeability associated with saturated hydraulic conductivity κ_S, and the values of κ_{FS} associated with K_{FS} that were fit using the analytical solution for the Green and Ampt model. The values of K_{FS} optimized to fit the Green and Ampt imbibition model in the analytical solution are 1.5 to 20.7 times lower than the K_S values determined by the falling head method. The greatest discrepancies are found in the coarsest materials (Table 4.1) and with n-hexane imbibing. The coarse sand results are as expected since wetting with upward imbibition leaves the largest pores air-filled, and thus lowering conductivity. In the case of the n-hexane, it appears that the lower contact angle gives rise to greater film flow and therefore, lower ultimate saturation, as was noted in water imbibition into previously water wet sand.

Looking at an alternative scenario, the independently measured falling head K_S values, which would hold if the media fully saturated behind the wetting front, were put into the Green and Ampt model leaving only the parameters h_f and t_0 to be optimized (Figures 4.1 through 4.4). The poor fitting results obtained using K_S versus the K_{FS} values, supports the conclusion that the actual hydraulic conductivity at the wetting front during imbibition, is indeed lower than the fully saturated conductivity of the sands.

Table 4.1 Calculated κ_S versus Fitted κ_{FS} for independently measured K_S and K_{FS} fitted by the dynamic method.

Sand	Solution	κ_S measured (cm^{-1})	κ_{FS} fitted (cm^{-1})	Ratio
40/50	n-hexane	[b]0.066	[c]0.028	2.40
	water	[a]0.065	[c]0.044	1.49
	$NaNO_3$	[b]0.065	[c]0.032	2.02
30/40	n-hexane	[b]0.118	[c]0.032	3.63
	water	[a]0.116	[c]0.072	1.62
	$NaNO_3$	[b]0.116	[c]0.050	2.35
20/30	n-hexane	[b]0.233	[c]0.030	7.78
	water	[a]0.230	[c]0.108	2.12
	$NaNO_3$	[b]0.230	[c]0.078	2.95
12/20	n-hexane	[b]0.487	[c]0.024	20.65
	water	[a]0.480	[c]0.103	4.64
	$NaNO_3$	[b]0.480	[c]0.122	3.95

[a]As measured via falling head method (Section 2.2.4).
[b]As calculated using the intrinsic permeability (Section 2.2.5).
[c]As fitted using the Green and Ampt model (Section 2.3.4). Mean of three repetitions with acceptable standard deviation range of 0.002 to 0.039.

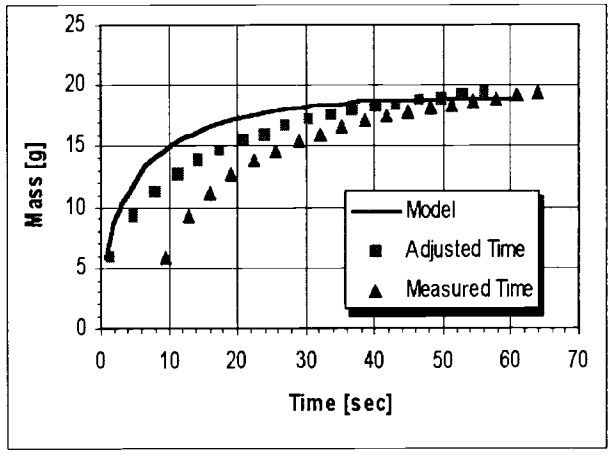

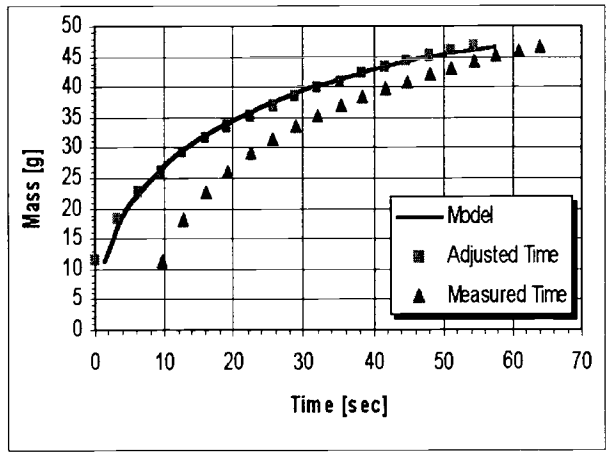

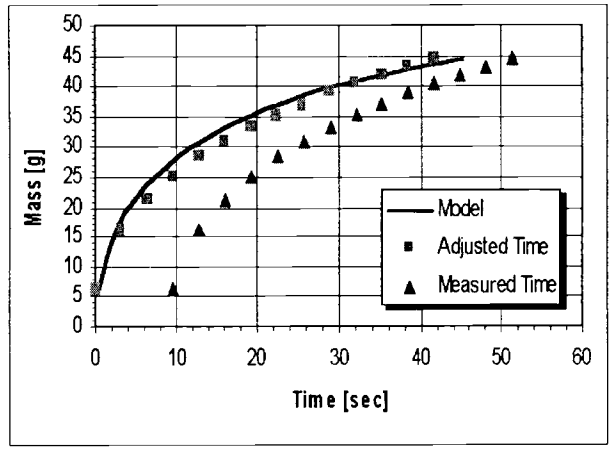

Figure 4.1 Imbibition of n-hexane, pure water, and salt solution respectively into 40/50 grade sand. Measured falling head K_S values are used in the Green and Ampt Model, requiring the model to optimize only h_f and t_0.

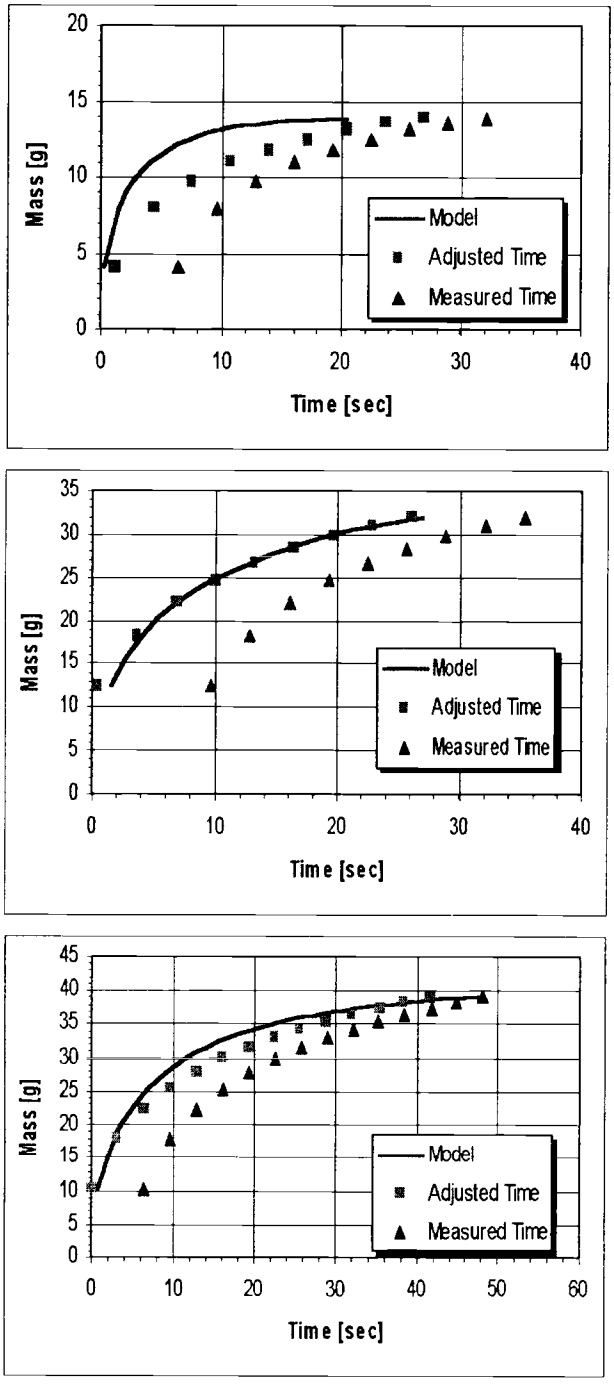

Figure 4.2 Imbibition of n-hexane, pure water, and salt solution respectively into 30/40 grade sand. Measured falling head K_S values are used in the Green and Ampt Model, requiring the model to optimize only h_f and t_0.

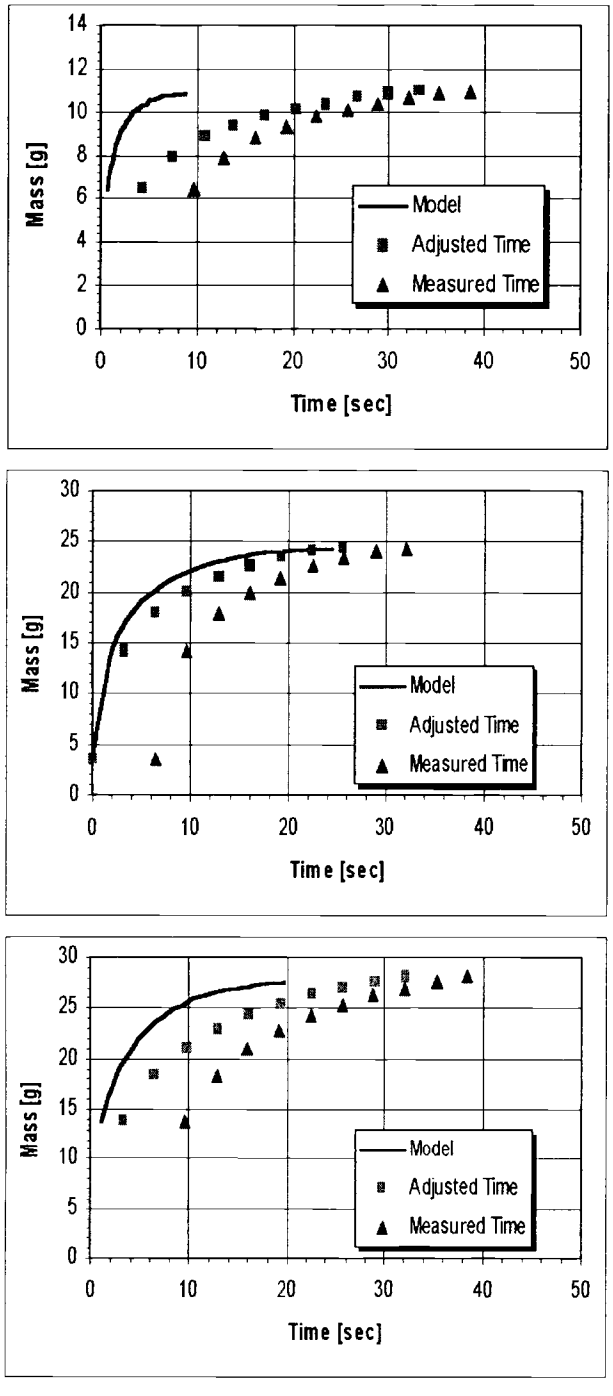

Figure 4.3 Imbibition of n-hexane, pure water, and salt solution respectively into 20/30 grade sand. Measured falling head K_S values are used in the Green and Ampt Model, requiring the model to optimize only h_f and t_0.

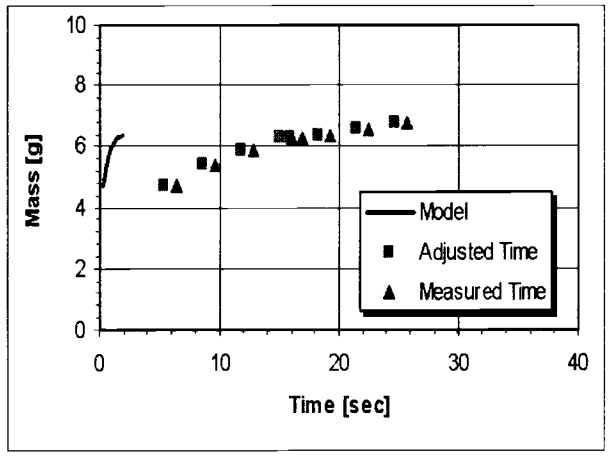

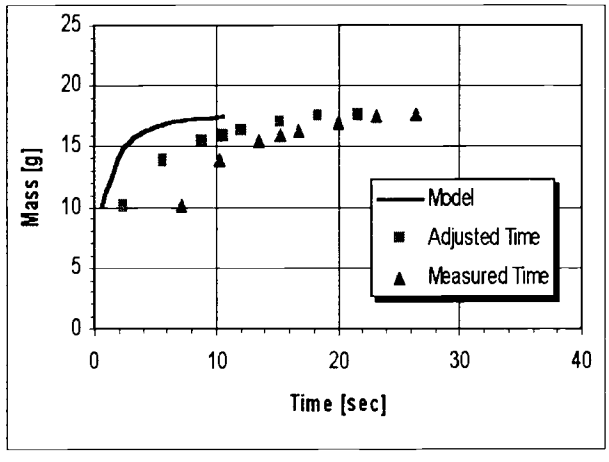

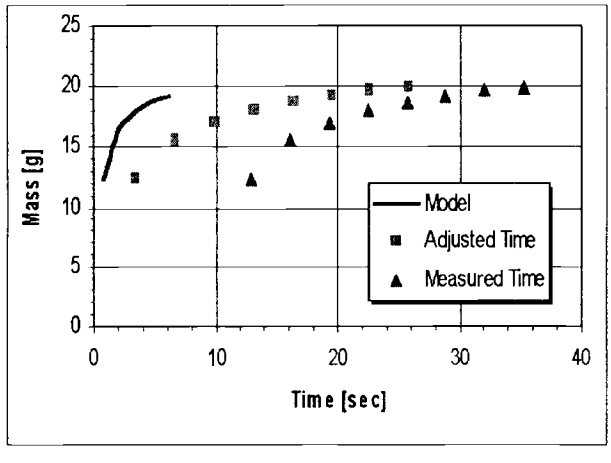

Figure 4.4 Imbibition of n-hexane, pure water, and salt solution respectively into 12/20 grade sand. Measured falling head K_S values are used in the Green and Ampt Model, requiring the model to optimize only h_f and t_0.

The fit between the model and the adjusted data for the 40/50 grade sand is quite good, especially for imbibition of water (Figure 4.1). The salt solution test in Figure 4.1 also results in a close fit, however the n-hexane results deviate, reflecting the higher ratio shown in Table 4.1. The same holds for water imbibing into 30/40 grade sand (Figure 4.2), but the differences between K_S and K_{FS} are more significant in the two larger sand grades (Figures 4.3 and 4.4). As the media becomes coarser, its effective pore radius becomes larger. The geometry of the pores, specifically the body radii, dictates the filling pressure head h_f, while the emptying pressure head is determined by size of the pore necks (Selker et al., 1999). The "ink bottle" effect as described by (Hillel, 1998) can help explain this phenomenon. The hypothetical pore shown in Figure 4.5, consists of the pore body having a larger radius r_b, interconnected with other pores by narrow channels known as the pore necks having radius r_n. Since the media is initially dry during imbibition, the analytical model optimizes a lower value for hydraulic conductivity. The pores are filled with air, which is being forced out, we assume, of all available pore space. During the measured hydraulic conductivity tests, the sands are fully saturated resulting in a continuous hydraulic connection from pore to pore. The coarser sand grades have larger pores, which require a higher pressure potential to fill them as r_b is increasing from the finest sand grade (40/50) to the coarsest (12/20). Since the sand is initially dry, the interface at the wetting front is actually overcoming these pressure potential boundaries, resulting in a lower hydraulic

conductivity represented by K_{FS}. This further supports that the media is not fully saturated at the wetting front interface during imbibition.

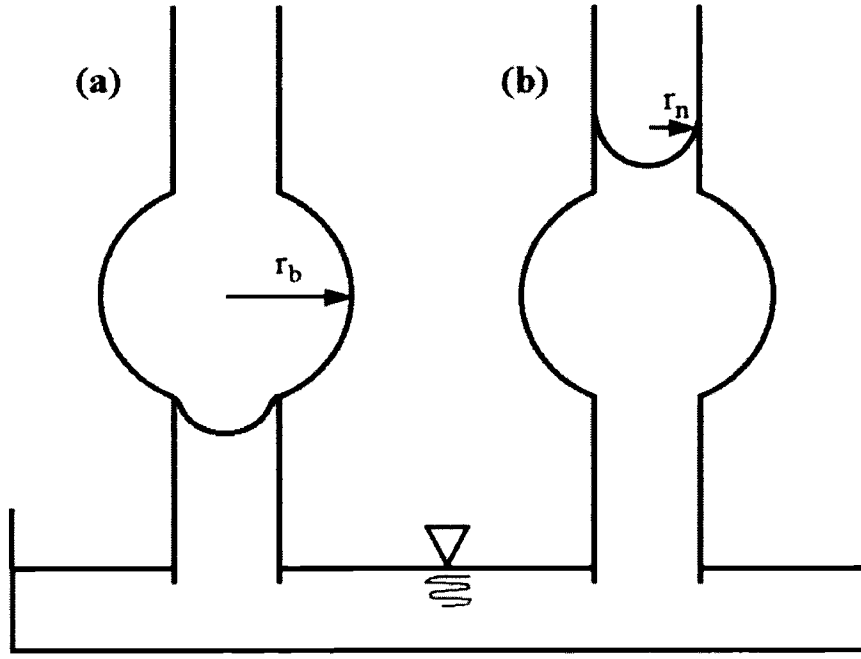

Figure 4.5 The "ink bottle" effect which determines the equilibrium height of water in a variable width pore: (a) capillary rise (sorption) and (b) capillary drainage (desorption). From Hillel (1998).

One of the key assumptions of the Green and Ampt theory of infiltration into dry soils is that the soil is completely saturated up to a sharp, well-defined wetting front (Figure 4.6). The analyzed data, however, suggest that this is not the case. The analytical solution presented by Brooks and Corey (1964) for determining the degree of saturated hydraulic conductivity at any given water content was given in Section 2.3.4. Because K_{FS} represents the hydraulic conductivity at some degree of

saturation, our $K(\theta)$ term from the Brooks and Corey solution is therefore the same as our K_{FS} determined by the modified Green and Ampt model. Full saturation θ_S is taken from Table 2.4. Residual saturation θ_0 and the fitting parameter λ were taken from Schroth et al. (1996). Table 4.2 summarizes the values calculated for θ_{fs}, related to the optimized K_{FS} using the parameters also specified in the table.

Table 4.2 Degree of saturation θ_{fs} for fitted K_{FS}.

	40/50	30/40	20/30	12/20
[a]K_{FS} (cm/sec)	0.043	0.071	0.107	0.102
[b]K_S (cm/sec)	0.065	0.115	0.228	0.476
[c]λ	6.17	6.91	5.57	3.94
[d]η	3.324	3.289	3.359	3.508
[e]θ_S (cm^3/cm^3)	0.337	0.328	0.330	0.324
[c]θ_0 (cm^3/cm^3)	0.020	0.018	0.016	0.012
[f]θ_{fs} (cm^3/cm^3)	0.300	0.286	0.267	0.211

[a]As fitted by the modified Green and Ampt solution (Table 3.4).
[b]As measured using the falling head method (Table 3.1).
[c]As reported by Schroth et al., (1996).
[d]As calculated by Brooks and Corey (1964) in Equation 4.1.
[e]Average value based on the porosity of three packed columns per each of the four sand grades as prepared for the experiments and reported previously in Table 2.4.
[f]Degree of saturation θ_{fs} for K_{FS} fitted by the modified Green and Ampt solution, calculated using Equation 4.2 and parameters in Table 4.2.

The computed degree of saturation behind the wetting front θ_{fs} is between 20% and 30% for the four grades of Accusand® as given by Table 4.2. This challenges the assumption that the column is fully saturated up to the wetting front (Figure 4.6). Using the residual saturation θ_0 and the fitting parameter λ, formerly

determined for the same sands by Schroth et al. (1996), was justified due to the fact that our measured degree of residual saturation for similarly packed 40/50 degree sand columns were close (mostly between 1% and 2%) as shown in Figure 3.15. Full saturation θ_S values were also very close to those determined by Schroth et al. (1996) within a 1% to 2% difference across all four sand grades, as shown in Table 2.4. Deviations from the parameter values determined by Schroth et al. (1996) did not have any notable effect on the calculation of θ beyond 1%.

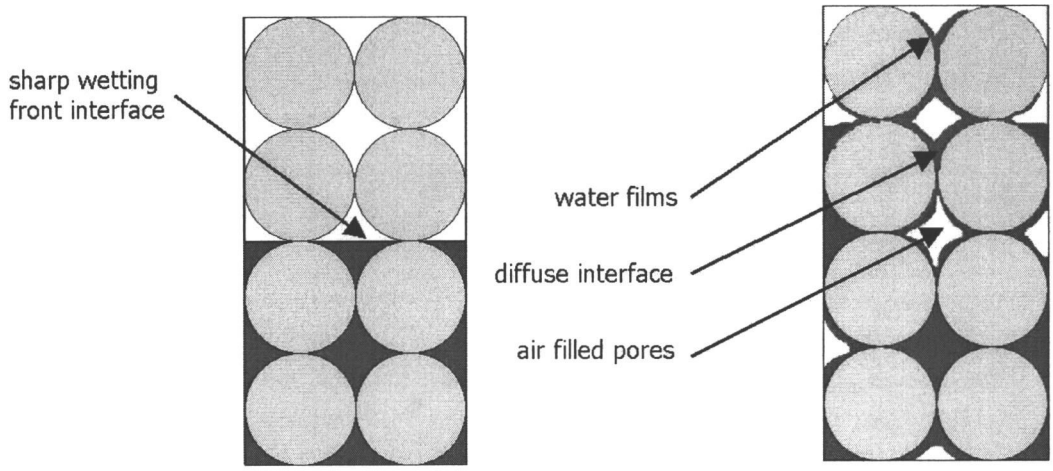

Figure 4.6 The sharp wetting front assumed by the Green and Ampt theory on the right. A more likely scenario illustrating the wetting front is depicted on the left.

4.3 STATIC METHOD VS. DYNAMIC METHOD

Our experimental results suggest that dynamic contact angles can deviate significantly from their static values, consistent with the observation of previous studies (Blake, 1993). In recognition of the temporal effects, Meyers (1991) refers to the contact angle of a moving wetting line as a dynamic contact angle. A static method is one in which the processes involved with imbibition are deemed to have stabilized or come into equilibrium, after which the contact angle is calculated via Equation 2.6. In many practical applications, the wetting phenomena of interest are "dynamic" in nature, involving a moving wetting line at which equilibrium is never attained (Meyers, 1991). Resulting contact angles summarized in Table 4.3 comparing the methods are as expected in accordance with definitions of static and dynamic contact angles. The similarity between the contact angle for pure water and the saline solution in dry sand (particularly in the static method results), despite their different surface tensions is also as expected. Indeed, Weisbrod et al. (submitted b) found that the higher contact angle of the saline solution had no impact on fingering in air-dry silica sand. Static properties are intrinsic to the material itself and are unaffected by any external variables, while dynamic properties are manifested in the response of the body to externally imposed effects such as fluid fluxes (water and air), energy fluxes (radiant or convective), and mechanical stresses tending to cause deformation and failure (Hillel, 1998). Static contact angles should be expected to be smaller than those measured in a dynamic system because the dynamic contact angle is dependent on the speed and direction

of the wetting front. Although some speed-independent regimes have been reported, the experimentally observed contact angle γ is usually found to depend on both the speed and direction of wetting line displacement, that is, γ is velocity-dependent, as illustrated in Figure 4.7 (Blake, 1993). The advancing contact angle in a dynamic system can be greater or lesser depending on the velocity of the fluid infiltrating the system. The greater velocity pushes the fluid forward, increasing the contact angle of that fluid on the solid surface. The situation is made more complex by the fact that even the static contact angle is unlikely to be single-valued. In most real systems, the value observed when the wetting line is apparently stationary depends on the history of the system and varies according to whether the wetting line is tending to advance or recede (Blake, 1993).

In comparing the h term between the two methods we see that the values in Table 4.3 show a higher h in the static system. This h represents height of rise at equilibrium while the h term in the dynamic method is the pressure potential h_f at the wetting front as explained in Section 2.1.3. Among the four sand grades, the effective pore radii between the static and dynamic methods differ slightly in that the dynamic method predicts a smaller effective pore radius (e.g., lower capillarity or greater contact angle). It is interesting to note the close proximity of values for r between the two methods.

Miller and Miller (1956) presented a comprehensive methodology with which to extend information between geometrically similar pairs of porous media systems. Typically, it is assumed that if the particle size distributions are linearly

related (that is, two particle size distributions will fall on one line if the particle dimensions of one are multiplied by the appropriate constant), and the porosities are the same, then the two media are similar in the sense of Miller and Miller (Selker et al., 1999). Schroth et al. (1996) demonstrated the Miller-similarity for the same grades of Accusand® for both static and dynamic properties. Thus we are able to extrapolate from one sand grade to another for it is well known that these sands are similar in the geometric sense. It is interesting to scale the results summarize in Table 4.3 in terms of water pressure. If we consider the Laplace equation (Equation 1.6) in terms of radius r:

$$P = \frac{2\sigma \cos\gamma}{r} \tag{4.1}$$

Now multiplying both sides of Equation 4.1 by $\frac{\lambda}{2\sigma \cos\gamma}$ yields

$$\frac{2\lambda}{r} = \frac{\lambda P}{2\sigma \cos\gamma} \tag{4.2}$$

The left side of the equation is constant for any similar medium; thus the terms on the right side must be constant as well. Scaled pressure can then be defined as

$$P_* = \frac{\lambda P}{2\sigma \cos\gamma} \tag{4.3}$$

Although we have kept the pressure notation, this could just as well be written in units of head, which we could write as h_*.

$$h_* = \frac{\lambda h}{2\sigma \cos\gamma} \tag{4.4}$$

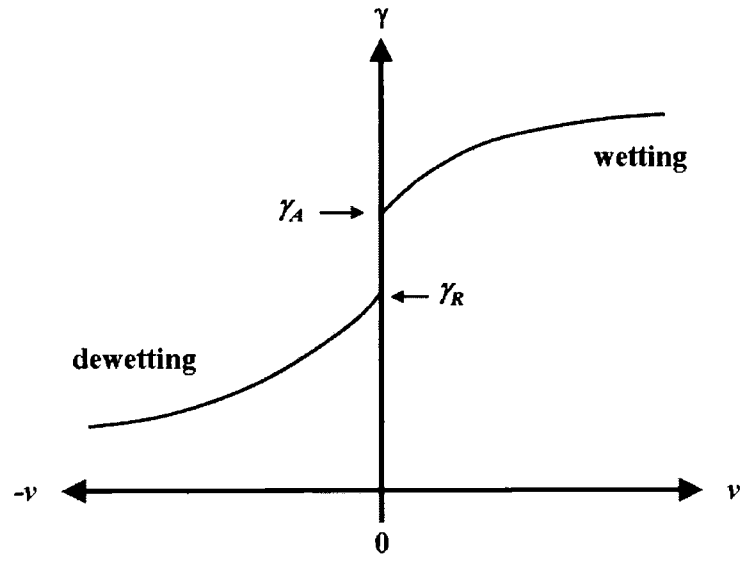

Figure 4.7 Schematic representation of the velocity dependence of the experimentally determined contact angle γ, showing static advancing and receding limits γ_A and γ_R (Blake, 1993).

Table 4.3 Static Method vs. Dynamic Method, Dry Sand.

Sand	Solution	Capillary rise, h (in cm)		Pore radius, r (in cm)		Contact angle (in degrees)	
		Static	Dynamic	Static	Dynamic	Static	Dynamic
40/50	n-hexane	6.68	7.71	0.009	0.007	0	0
	Pure water	16.20	13.27	0.009	0.007	23	49
	5 m $NaNO_3$	14.17	13.38	0.009	0.007	23	41
30/40	n-hexane	5.15	6.55	0.011	0.009	0	0
	Pure water	11.48	8.62	0.011	0.009	32	60
	5 m $NaNO_3$	10.04	9.36	0.011	0.009	33	52
20/30	n-hexane	3.68	6.01	0.016	0.010	0	0
	Pure water	8.22	6.43	0.016	0.010	32	66
	5 m $NaNO_3$	7.13	6.41	0.016	0.010	33	63
12/20	n-hexane	2.52	4.85	0.023	0.012	0	0
	Pure water	5.72	5.52	0.023	0.012	30	64
	5 m $NaNO_3$	4.99	4.57	0.023	0.012	31	66

After scaling pressure terms for both the static and dynamic methods, pressure head for all sand grades was scaled to that of the 40/50 grade sand. We can see that by simple Miller scaling, we can explain all but 16% of the variation in values, which differed from 265% to 284% in the raw data for the static method.

Table 4.4 Scaled pressure terms for static and dynamic methods.

		Static Method			Dynamic Method		
Sand	Solution	h	h_*	h_* scaled to 40/50	h_f	h_{f*}	h_{f*} scaled to 40/50
40/50	n-hexane	6.68	0.065	1.000	6.23	0.061	1.000
	Pure water	16.20	0.043	1.000	11.30	0.036	1.000
	5 molal $NaNO_3$	14.17	0.034	1.000	12.18	0.036	1.000
30/40	n-hexane	5.15	0.074	1.142	4.86	0.070	1.156
	Pure water	11.48	0.049	1.143	7.98	0.041	1.155
	5 molal $NaNO_3$	10.04	0.039	1.143	8.14	0.042	1.156
20/30	n-hexane	3.68	0.071	1.094	3.53	0.068	1.125
	Pure water	8.22	0.047	1.095	4.96	0.040	1.126
	5 molal $NaNO_3$	7.13	0.038	1.096	5.62	0.041	1.126
12/20	n-hexane	2.52	0.076	1.161	2.17	0.065	1.072
	Pure water	5.72	0.050	1.163	3.29	0.038	1.069
	5 molal $NaNO_3$	4.99	0.040	1.164	3.99	0.039	1.068

We can also use the same concept of Miller scaling to scale the effective pore radius of the sands based on their particle size distribution using the following relationship:

$$r_* = \frac{r}{\lambda} \tag{4.5}$$

Miller scaled values for static effective capillary radius, were within 12% of each other, explaining 70% of this variation observed. The radii from the dynamic tests did not scale well, with an increase in variability observed post-scaling. Using Equation 2.29 and the data of Table 4.1, the degree of saturation θ was calculated to be 0.268, 0.235, 0.189 and 0.146 for n-hexane imbibition into 40/50, 30/40, 20/30 and 12/20 sand grades respectively. Clearly each texture of sand reached unique degrees of saturation, and therefore the fluid geometries were not geometrically similar, violating the assumptions of scaling. Thus the calculated effective pore-capillary radius r reflects distinct conditions between the sand grades. Static method values for r scale well between the sand grades (Table 4.5). In the static method however, the porosity of the sample was taken to be θ_S (Table 2.3) rather than the optimized liquid content θ_{fs} as in the dynamic method.

4.4 COMPARISON OF DYNAMIC SOLUTIONS

The two dynamic methods employed were the Washburn Theory and the modified Green and Ampt approach. The former did not work with the four Accusand® grades, at least with the method utilized by (Rulison, 1996b), which is outlined in Section 2.1.2. The force of gravity is significant relative to capillary force, but is neglected in the Washburn theory as implemented by Rulison (1996b). Figure 4.8 illustrates an imbibition experiment run at Kruss Laboratories, USA, utilizing the Washburn theory. This particular experiment was conducted with fluids of low surface tension (e.g., Acetone, σ_{lg}=23.7 mN/m) and the porous media was a very

Table 4.5 Scaled pore radius r for the static and dynamic method for imbibition into dry sand.

		Static Method			Dynamic Method		
Sand	Solution	r	r_e	r_e scaled to 40/50	r_e	r_e	r_e scaled to 40/50
40/50	n-hexane	0.009	0.025	1.000	0.007	0.019	1.000
	Pure water	0.009	0.025	1.000	0.007	0.019	1.000
	5 molal $NaNO_3$	0.009	0.025	1.000	0.007	0.019	1.000
30/40	n-hexane	0.011	0.021	1.212	0.009	0.017	1.153
	Pure water	0.011	0.021	1.212	0.009	0.017	1.153
	5 molal $NaNO_3$	0.011	0.021	1.212	0.009	0.017	1.153
20/30	n-hexane	0.016	0.022	1.117	0.010	0.014	1.390
	Pure water	0.016	0.022	1.117	0.010	0.014	1.390
	5 molal $NaNO_3$	0.016	0.022	1.117	0.010	0.014	1.390
12/20	n-hexane	0.023	0.021	1.204	0.012	0.011	1.795
	Pure water	0.023	0.021	1.204	0.012	0.011	1.795
	5 molal $NaNO_3$	0.023	0.021	1.204	0.012	0.011	1.795

fine ground titanium oxide. The structure of this media would suggest that the effective pore radius is indeed very small, much smaller than that of the Accusand®. The data presented in Figure 4.8 shows the linear relationship needed to calculate the slope m_l^2/t as mentioned in Section 2.1.2. This linear relationship is expected for this fluid-media pair because the force of gravity is negligible relative to capillarity at this time scale.

When this method was applied to the Accusand®, results adequate to determine the contact angle were not obtained. When the raw data was plotted (Figure 4.9), a linear section was not evident, making it impossible to identify the required slope.

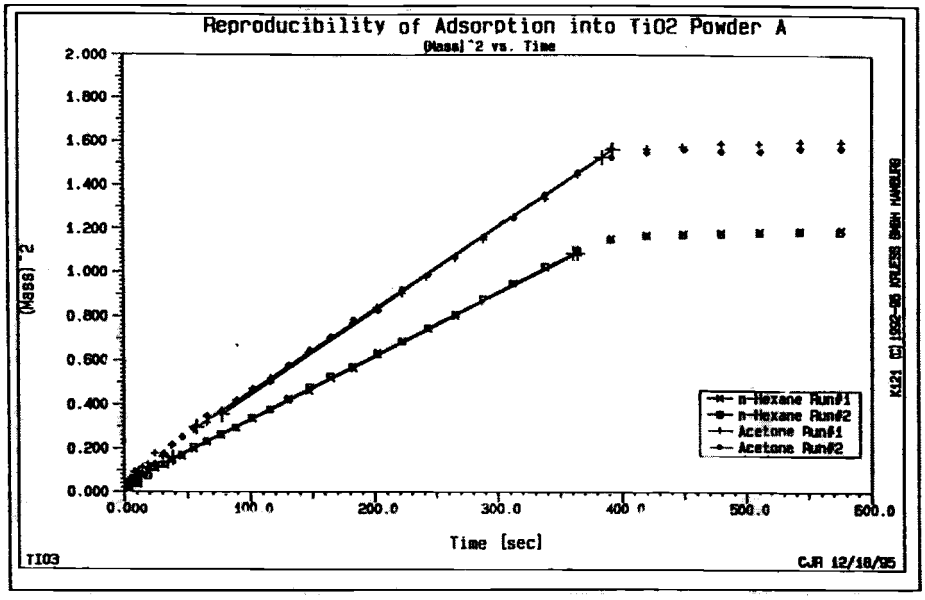

Figure 4.8 Imbibition data from a Washburn theory based experiment. The media used is a fine, Titanium Oxide powder and the imbibing fluids, both having low surface tension (18.4 mN/m and 23.7 mN/m respectively) are n-hexane and acetone (from Rulison, 1996b).

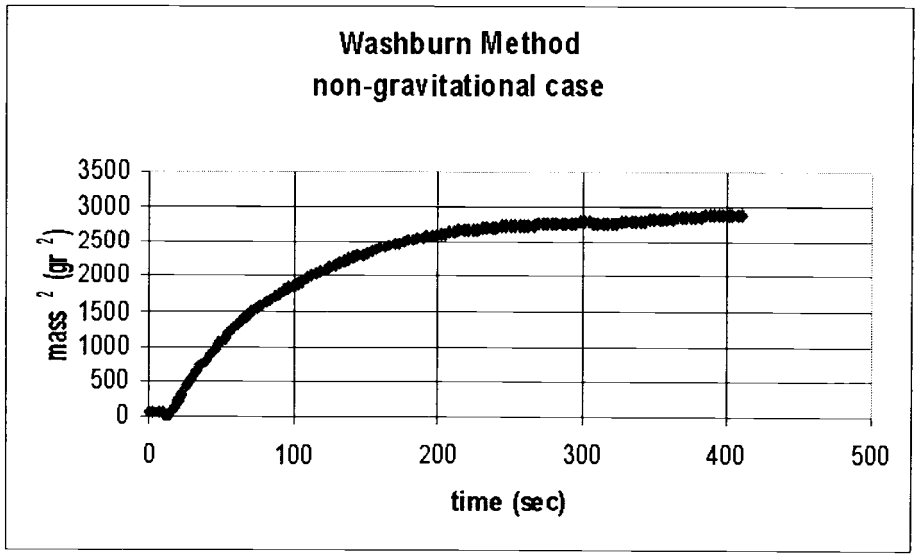

Figure 4.9 Imbibition data from an experiment conducted with 40/50 grade Accusand®. The imbibing fluid is pure water having a surface tension of 72.8 mN/m.

4.5 DRY SAND VS. PRE-WETTED SAND

Natural soils are rarely completely dry and therefore the experimental results from the idealized water imbibition into air-dried media have limited practical implications for natural systems. Therefore, comparing contact angle developed in air-dry sand to that into pre-wetted sand is of a special interest. Weisbrod et al. (submitted b), studied finger flow in air-dry versus pre-wetted Accusand® using pure water and 5 molal $NaNO_3$. They showed that the two solutions migrated similarly in air-dry sand suggesting that the different contact angle had no impact on fingering. A limited amount of work has been performed in regards to fingering into wetted media, and the effect of initial water content on finger development is not yet fully understood (de Rooij, 2000). It is usually assumed that a wetting fluid imbibing into a liquid coated porous media leads to a contact angle close to zero, and the imbibing fluid will freely wet the water coated particle surfaces. Therefore, we expected to see contact angles of near zero for water imbibition into water-wetted sand.

The contact angle of the 5 molal $NaNO_3$ solution into water-wetted sand, while greater than pure water into water-wetted sand, was also expected to be lower than into initially dry sand. Recently, Weisbrod et al. (submitted a) suggested that if the advancing fluid is a brine with high surface tension and the resident fluid is pure water, a temporary contact angle may developed. The authors noted that this might explain the finger-like shape of saline plumes applied into sand residually saturated with pure water.

Lu et al. (1994a and 1994b) showed that much less air was entrapped in an initially dry profile than in an initially wet profile, supporting the observation that a clearly defined, saturated, wetting front did not exist in the initially wet media. Initially wet media at residual saturation is fundamentally different than dry media in that a connected moisture film coats the grain surfaces. Continuous filling due to film flow combined with Haines jumps will occur during infiltration provided a continuous water film exists within the profile (Lu et al., 1994b). It appears that for low water saturations in coarse soils, near residual, Haines jumps dominate the infiltration process, while for higher saturations film flow becomes more important (Weisbrod et al., submitted a). The common assumption of a saturated wetting front cannot be used in pre-wetted sand. Weisbrod et al. (submitted b) showed that the degree of saturation at the fingertip never exceeds 27% in pre-wetted sand while it was about 80% to 90% once the same infiltration conditions were used in air-dry sand. Therefore, an attempt to calculate the capillary rise based on the total volume (Equation 2.3) imbibed into the column as obtained in the static experiments, may lead to major errors. For example if the average degree of saturation of the imbibing fluid is 30% rather than 100% the actual maximum capillary rise for a given volume is three times higher than the calculated one.

Assuming a zero contact angle when pure water is wetting the sand presaturated with pure water, we can infer the height h of capillary rise at equilibrium using Equation 1.8. Using the pre-wetted 40/50 grade Accusand® as an example, the calculated h value necessary to achieve a zero contact angle should be

16.62 cm. Referring to Table 3.6, we can see that the height h obtained by calculation based on the assumption of full saturation behind the wetting front (Equation 2.3), yielded a capillary height of 12.50 cm (based on a average of three repetitions). Considering the relationship that Brooks and Corey (1964) proposed between h and θ, we see that for a height h less than the pressure potential h_f for a specific soil, the relationship between h and θ is shown in the following equation

$$\frac{\theta - \theta_0}{\theta_S - \theta_0} = \left(\frac{h_f}{h}\right)^{\lambda} \tag{4.3}$$

Solving equation 4.3 in terms of θ yields

$$\theta = \left(\frac{h_f}{h}\right)^{\lambda} (\theta_S - \theta_0) + \theta_0 \tag{4.4}$$

Using this equation, the parameters from Table 4.2, and the h needed to achieve a near zero contact angle (16.62 cm), the degree of saturation θ necessary to achieve the height h was calculated at 82%. Therefore, it appears that diffuse capillary imbibition, lacking a distinct wetting front, was controlling the infiltration process in the pre-wetted sand, in agreement with Weisbrod et al. (submitted b).

Specifically, looking at the terms h and γ in Table 4.6 we see that the apparent capillary rise h was lower in the pre-wetted sand, and the apparent contact angle γ was in fact higher. We expect that this behavior is due to our use of porosity for Φ in the static case, which was seen to be violated severely in pre-wetted sands through careful analysis of dynamic results (Table 3.7). The dynamic method

results summarized in Table 4.7 illustrate an expected deviation in both terms, h_f and γ, between the dry and pre-wetted sand experiments.

Table 4.6 Dry vs. Pre-wetted Sand, static method.

Sand	Solution	Capillary rise, h (in cm)‡		Pore radius, r (in cm)‡		Contact angle (in degrees)‡	
		Dry	Wet	Dry	Wet	Dry	Wet
40/50	n-hexane	6.68	†	0.009	0.009	0	†
	Pure water	16.20	12.50	0.009	0.009	23	45
	5 m $NaNO_3$	14.17	10.81	0.009	0.009	23	46

† n-hexane was not used to imbibe into pre-wetted sand.
‡ Dry results from Table 3.3 and pre-wetted results from Table 3.6.

Table 4.7 Dry vs. Pre-wetted Sand, dynamic method with 40/50 sand

Solution	Capillary rise, h (in cm)‡		Pore radius, r (in cm)‡		Contact angle (in degrees)‡		κ_{FS} (cm/sec)‡	
	Dry	Wet	Dry	Wet	Dry	Wet	Dry	Wet
n-hexane	7.71	†	0.007	0.007	0	†	0.028	0.027
Pure water	13.27	20.27	0.007	0.007	49	2	0.044	0.006
5 m $NaNO_3$	13.38	16.62	0.007	0.007	41	21	0.032	0.006

† n-hexane was not used to imbibe into pre-wetted sand.
‡ Dry results from Table 3.4 and pre-wetted results from Table 3.7.

Factors influencing this unexpected phenomenon can most likely be attributed to the h term of the equation representing height of capillary rise into porous media. This term is calculated on a volume basis of the imbibed solution (Equation 2.3) in

the static method for both initially dry and pre-wetted sands. While the assumption made in Section 2.1.1 associated with Equation (2.3) hold for initially dry sand, it does not appear to holds for the pre-wetted sand. Hysteresis plays an important role here. The pre-wetted sand, which has been fully saturated and then drained to residual saturation, leaves a portion of the pore space encapsulated with air, isolated by the residual water (Figure 4.10). Lower water content upon imbibition due to reduced available pore space results in a higher computed value for h upon

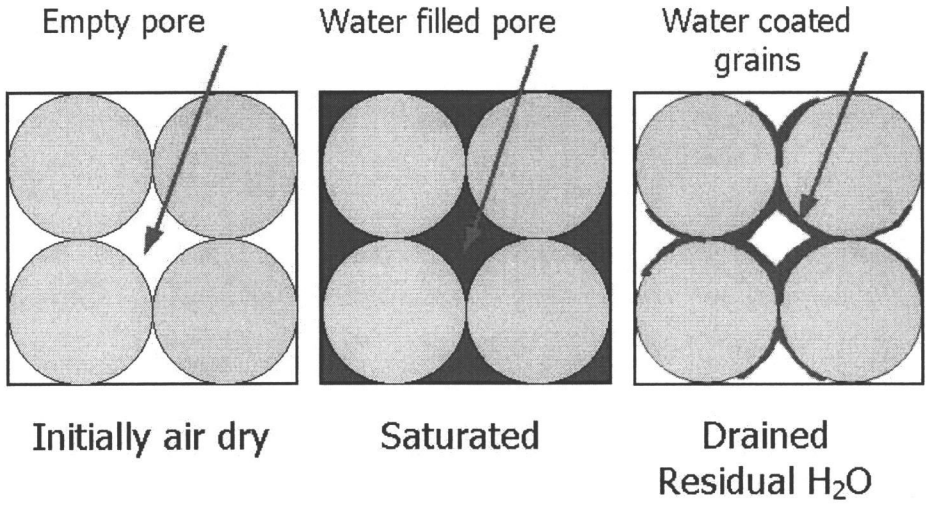

Figure 4.10 Uniformly packed, dry, spherical sand grains are saturated and drained until only residual water remains coated on the grains. This residual water traps air, isolating certain pores. This pre-wetted sand not only reduces effective pore space, but also affects the wetting process by increasing height of capillary rise thus reducing the contact angle.

reaching an equilibrium state after imbibition of the solution into pre-wetted sand. The contact angle is reduced to near zero, by the Young-Laplace theory in Equation

1.3, making the sand more wettable by the imbibing fluid. Combined with the isolated pores, these conditions should push the height of rise much higher than that observed in dry sand. Besides the inability to calculate the height of rise volumetrically, another barrier was created by the physical height of the sand columns. The static columns were only 25.0 cm high, which is easily exceeded during the 24-hour imbibition period based on the retention curve for 40/50 grade Accusand® (Figure 4.11). The wetting front becomes difficult to delineate as the height of rise increases into the pre-wetted media, however we know from previous work by Schroth et al., (1996) and Niemet and Selker (2001), that the capillary fringe for this particular grade of Accusand®, exceeds 25.0 cm.

The dynamic method however, optimized the pressure potential h_f which yielded a near zero contact angle for water imbibition into pre-wetted sand (Table 4.7). By using the Brooks and Corey relationship, conditions were optimized based on effective pore space, which changes when initially air-dried sand is saturated and allowed to drain to hydrostatic equilibrium. Most critical for these data is whether the saline-fresh water contact angle agreed with the simple force balance shown in Figure 1.4. Using Equation 4.6, one would expect to calculate a zero degree contact angle in the case of water imbibing water-wetted media, and a contact angle of 25° in the case of the saline solution imbibing into water-wetted media. These results presented in Table 4.7, are essentially identical to these predictions.

For the case of our pre-wetted sands, Equation 1.2 essentially becomes

$$\sigma_{sg\,water} + \sigma_{sl} = \sigma_{sl} + \sigma_{\lg\,saline} \cos\gamma \tag{4.5}$$

where the solid/gas interface is now coated with a water film, and we have two interfacial forces σ_{sl} opposing one another, due to the water-wetted solid surface of the sand grains. Equation 4.5 then reduces to Equation 4.6 with the opposing σ_{sl} forces canceling each other yielding

$$\gamma = \cos^{-1}\left(\frac{\sigma_{\lg\,water}}{\sigma_{\lg\,saline}}\right) \tag{4.6}$$

where the surface tension of pure water, which is used to wet the sand, is over the surface tension of the imbibing solution, in this case, the saline solution (5 molal $NaNO_3$). The theorized force balance relationship for a water-wetted, solid surface is illustrated in Figure 4.12.

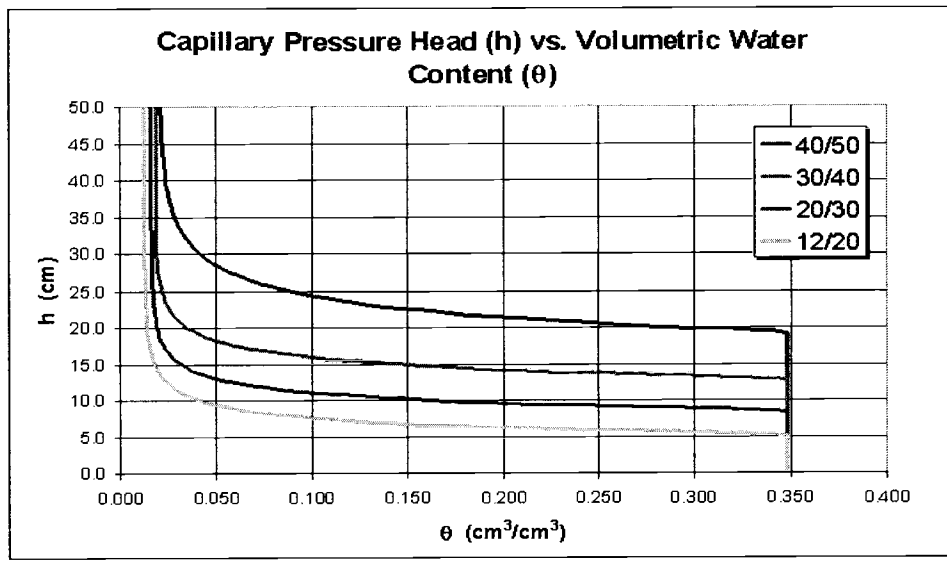

Figure 4.11 Water retention curves as obtained by Schroth et al., (1996) for the four grades of Accusand®.

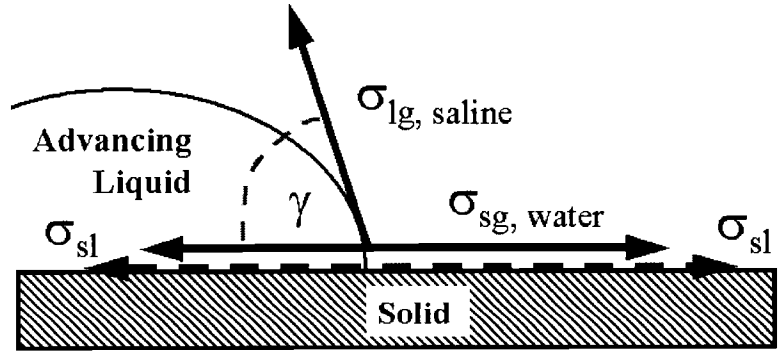

Figure 4.12 Three-phase line of contact between forces. Here σ_{sg} is the relative surface tension between a liquid and the gas when the media is water wetted, σ_{lg} is the relative surface tension between the liquid and the gas of the imbibing solution (here 5 molal $NaNO_3$), and σ_{sl} is the relative surface tension between the solid and the liquid, now acting in opposite directions since the sand grains are coated with a water film.

5 CONCLUSION

Wettability of porous solids, while not obtainable by optical inspection, can be estimated using methods based on capillary models of imbibition. Our methods, both static and dynamic, demonstrated their ability to estimate the contact angle formed by solutions of varying surface tension on silica sands. The contact angle of the imbibing solutions was estimated in both dry and water-wetted sand using an analytical method, based on the Green and Ampt theory, as an effective method for estimating the contact angle of imbibing fluids into dry and pre-wetted sandy soils. The model incorporates the observed lack of complete saturation using the retention/conductivity model of Brooks and Corey (1964) to calculate the effective degree of saturation during imbibition based on the optimized hydraulic conductivity.

The estimated contact angles in the static and dynamic methods were compared for dry sand, showing that dynamic contact angle measured higher for both pure water and 5 molal $NaNO_3$ imbibition. Comparison between the dynamic solution proposed by Rulison (1996b) based on Washburn's theory and the Green and Ampt based model for upward imbibition showed that gravity cannot be neglected in coarse porous media such as sand.

Independently measured hydraulic conductivity K_S, which was 1.5 to 20.7 times higher than the fitted conductivity values, was used as a fixed parameter in the Green and Ampt imbibition model so that the model optimized only two parameters (h_f and t_0). With this constraint, the model could not fit the data,

suggesting incomplete wetting. The degree of media saturation in the dynamic tests, calculated using the Brooks and Corey (1964) relationship, ranged from 21% to 30%.

Height of capillary rise plays a major role in pre-wetted sand. The imbibing fluids into the pre-wetted sand columns during static method tests lacked an apparent distinct wetting front. In the static method, calculation of capillary rise was based on the volume of liquid imbibed, yielding smaller capillary rise in the pre-wetted sand than in initially dry sand. However, a greater height of rise in pre-wetted sand is necessary to form the zero contact angle expected for pure water imbibition into water-wetted sand. The infiltration process is apparently dominated by diffuse capillary imbibition and restrictions imposed by the height of the samples. The results of the dynamic imbibition of water-wetted sand revealed apparent contact angles of 2° for water and 21° for 5 molal $NaNO_3$, which is very close to the 0° and 25° calculated using Young's equation (Equation 4.6). To my knowledge, this is the first observation of a contact angle effect observed between two miscible fluids.

The observed data suggest that the zero contact angle assumption is a poor one for clean dry silica sand. In a dynamic system, the effects caused by gravitational forces cannot be ignored in course porous media. Both methods estimated reproducible and reasonably consistent values of contact angle.

BIBLIOGRAPHY

Bauters, T. W. J., T.S. Steenhuis, D.A. DiCarlo, J.L. Nieber, L.W. Dekker, C.J. Ritsema, J.-Y. Parlange, and R. Haverkamp (2000). "Physics of water repellent soils." Journal of Hydrology 231-232: 233-243.

Blake, Terence. D. (1993). Dynamic Contact Angles and Wetting Kinetics. Wettability. J. C. Berg. New York, Marcel Dekker, Inc. 49: 50.

Brooks, R. H. and A. T. Corey (1964). Hydraulic properties of porous media. Ft. Collins, Colorado State University.

de Rooij, G. H. (2000). "Modeling finger flow of water in soils owing to wetting front instability a review." J. Hydrol 231-232: 277-294.

Fisher, Leonard R. and Prosper D. Lark (1979). "An Experimental Study of the Washburn Equation for Liquid Flow in Very Fine Capillaries." Journal of Colloid and Interface Science 69(No. 3): 486-492.

GJPO (1996). Vadose Zone Characterization Project at the Hanford Tank Farms. SX Tank Farm Report. Grand Junction, CO, US Department of Energy, Grand Junction Projects Office.

Green, T. R. and G. A. Ampt (1911). "Studies on soil physics: I. Flow of air and water through soils." J. Agric. Sci. 4: 1-24.

Haines, B. W. (1930). "Studies in physical properties of soil: 5. The hysteresis effect in capillary properties, and the modes of moisture distribution associated therewith." J. Agric. Sci. 20: 97-116.

Hillel, Daniel (1998). Environmental Soil Physics. San Diego, Academic Press.

Klute, A. and C. Dirksen (1986). Methods of Soil Analysis. SSSA Book. Madison, Soil Science Society of America.

Letey, J., M. L. K. Carrillo, and X. P. Pang (1999). "Approaches to characterize the degree of water repellency." Journal of Hydrology 231-232: 61-65.

Letey, J., J. Osborn, and R. E. Pelishek (1962). "Measurement of Liquid-Solid Contact Angles in Soil and Sand." Soil Science 93: 149-153.

Lu, T. X., J. W. Biggar, D. R. Nielsen (1994a). "Water movement in glass bead porous media, I. Experiments of capillary rise and hysteresis." Water Resour Res 30: 3275-3281.

Lu, T. X., J. W. Biggar, D. R. Nielsen (1994b). "Water movement in glass bead porous media, 2. Experiments of infiltration and finger flow." Water Resour Res 30: 3283-3290.

Malik, R. S., C. H. Laroussi, and L. W. DeBacker (1979). "Experimental Investigation of the Penetration Coefficient in Capillary Tubes." Soil Science 127 (No. 4): 211-218.

Marmur, A. (1992). Penetration and Displacement in Capillary Systems. Modern Approaches to Wettability. M. E. Schrader and G. I. Loeb. New York, Plenum Press: 327-356.

Meyers, D. (1991). Surfaces, Interfaces, and Colloids: Principles and Applications. New York, VCH Publishers, Inc.

Miller, E. E. and R. D. Miller (1956). "Physical theory for capillary flow phenomena." J. Appl. Phys. 27: 324-332.

Niemet, M. R., and J. S. Selker (2001). "A new method for quantification of liquid saturation in 2D translucent porous media systems using light transmission." Adv. Water Res. 24: 651-666.

Ouyang, Y. and C. Zheng (1999). "Density-driven transport of dissolved chemicals through unsaturated soil." Soil Sci 164: 376-390.

Rulison, Christopher (1996a). A Practical Comparison of the Techniques Used to Measure Contact Angles for Liquids on Non-Porous Solids. Charlotte, NC, Kruss USA.

Rulison, Christopher (1996b). Wettability Studies for Porous Solids Including Powders and Fibrous Materials. Charlotte, NC, Kruss USA.

Schaffer, Erik and Po-zen Wong (2000). "Contact line dynamics near the pinning threshold: A capillary rise and fall experiment." Physical Review 61 (5): 5257-5277.

Schroth, M. H., S. J. Ahearn, J. S. Selker and J.D. Istok (1996). "Characterization of Miller-Similar Silica Sands for Laboratory Hydrologic Studies." Soil Science Society of America 60 (no. 5): 1331-1339.

Selker, John S., C. Kent. Keller, and James T. McCord (1999). Vadose Zone Processes. Boca Raton, FL, CRC Press, LLC.

Selker, J. S. and M. H. Schroth (1998). "Evaluaton of hydrodynamic scaling in porous media using finger dimensions." Water Resources Research 34 (No. 8): 1935-1940.

Tillman, R. W., D.R. Scotter, M.G. Wallis, and B.E. Clothier (1989). "Water-repellency and its measurement by using intrinsic sorptivity." Aust. J. Soil Res. 27: 637-644.

Washburn, E. W. (1921). "The Dynamics of Capillary Flow." Physical Review 17: 273.

Watson, C. L., and J. Letey (1970). "Indices for characterizing soil-water repellency based upon contact angle-surface tension relationships." Soil Sci. Soc. Am. Proc. 34: 841-844.

Weisbrod, Noam., Michael R. Niemet, Mark L. Rockhold, Thomas McGinnis, and John Selker (submitted a). "Infiltration of saline solutions into variably saturated porous media." Water Resources Research.

Weisbrod, Noam., Michael R. Niemet, and John S. Selker (submitted b). "Imbibition of Saline Solution into dry and pre-wetted porous media" Advances in Water Resources.

Yang, X. F. (1995). "Equilibrium contact angle and intrinsic wetting hysteresis." Appl. Phys. Lett. 67 (No. 15): 2249-2251.